HELSINKI UNIVERSITY OF TECHNOLOGY
Faculty of Electronics, Communications and Automation
Department of Micro- and Nanosciences

Amit Khanna

CHARACTERIZATION OF SILICON MICRO-OPTICAL WAVEGUIDES

Master's thesis submitted in partial fulfillment of the requirements for the degree of Master of Science in Technology.

Espoo, Aug 15, 2008.

Supervisor: Seppo Honkanen, Prof.
Instructors: Antti Säynätjoki, D. Sc.

ACKNOWLEDGEMENTS

The following report is an extended work of an assignment in Optoelectronics pursued in the academic year 2006-07, supervised by Mikaël Mulot (Phd, Research Scientist, TKK/VTT) from whom I believe to have imbibed much energy.

I would like to thank Prof. Seppo Honkanen for giving me this opportunity to work in the Photonics Group, in the Department of Micro and Nanosciences, and the various motivating conversations.

To Antti Säynätjoki (D.Sc.) I owe special mention for being helpful and patient especially while I jostled with the, *not so*, trivial aspects of the study. I appreciate Markku Kapulainen (M.Sc.) for sparing time, resources and his unhurried approach. I also thank my colleagues for an easy atmosphere and sharing their expertise which has led to more ideas. I also appreciate the kindness of the staff at VTT Photonics laboratory for allowing me to use the laboratory resources and trusting my skills.

Finally, I thank my parents for the years of care and encouragement and gratitude for Mr. J.L. Khanna (*dadaji*) and Mrs. R.R. Khanna (*dadimaa*), my grandparents. Amidst the heaviness of it all, I thank my two sisters and friends for various lighter moments and joys.

Espoo, 15.08.2008.

Amit Khanna

HELSINKI UNIVERSITY OF TECHNOLOGY **ABSTRACT OF THE FINAL PROJECT**

Author:	Amit Khanna	
Title of thesis:	Characterization of Silicon Micro-Optical Waveguides	
Date:	Aug 15, 2008	**Pages:** 54
Faculty:	Electronics, Communication and Automation	
Professorship:	Photonics	**Code:** S-104
Supervisor:	Seppo Honkanen, Prof.	
Instructor:	Antti Säynätjoki**,** D. Sc.	

In modern electronic circuitry, electrical interconnects have not kept pace with increasing electronic processing speed. Various drawbacks of electrical domain viz. bandwidth limitation, signal delay, electromagnetic wave phenomenon propelled the use of optical fibers. Optical waveguides provide a novel solution because of the absence of these phenomena in the optical domain. Various materials like polymers, III-V semiconductor compounds, $LiNbO_3$ etc. have been analyzed for fabricating optical waveguides. We have chosen silicon as a material for optical waveguides. Silicon is extensively used for complimentary metal oxide semiconductor (CMOS) transistor fabrication. Thus, to use silicon for fabricating optical components is highly favorable from a technological standpoint.

In this thesis, we characterize silicon optical waveguides. Loss in 10μm wide hydrogenated amorphous silicon (a-Si:H) strip optical waveguides is estimated to be 1.5dB/cm and 0.1dB/cm in rib type silicon on insulator (SOI) optical waveguides. Reflectivity of Bragg mirror on a-Si:H strip waveguides is in the range 49-86%. We measured 0.5-1dB loss per etched mirror section for fundamental transverse electric (TE) and transverse magnetic (TM) modes propagating in SOI rib waveguide. A setup to measure birefringence in optical waveguides is discussed and its results are analyzed.

Ellipsometry of 260nm thick layer of a-Si:H, deposited by plasma enhanced chemical vapor deposition (PECVD), is done to ascertain the material refractive index. Spectral behavior of a-Si:H waveguides using a supercontinuum source is also studied.

Keywords: silicon, optics, silicon photonics, attenuation, Bragg mirror, birefringence, transmission spectrum, amorphous silicon, strip waveguides, SOI waveguides

Table of Contents

1. Introduction

Silicon is a ubiquitous material in electronic components and man-made micro-nano structures. High interest of industry and academia has led to advanced silicon processing techniques. These processing techniques resulted in an integrated electronic circuit (IC) technology utilized to bulk produce application specific integrated electronic circuits (ASIC) which are the backbone of the electronic industry today. Advantages of accurate silicon processing techniques are not limited to ASICs – also leading to demonstrations of a plethora of micro-electro-mechanical structures (MEMS) and micro-opto-electro-mechanical structures (MOEMS). These micro structures add real time sensing to the ICs as a result devices like lab-on-chip are now fabricated commercially for sensing in medicine, meteorology etc. New disciplines like Bio-MEMS, NEMS, (nano-electro-mechanical structures) etc. are being investigated. Owing to diversifying applications and maturing fabrication processes, silicon based micro-nano device technology is expected to grow in prominence. It may be apt to term this in the succession of '–lithic' ages as the 'silicon age'.

The gamut of nanotechnology has progressed as a consequence of sustained investor faith resulting from a positive feedback provided by advancing fabrication techniques and limitations of machines in market like size, functionality, portability, cost etc. Advancement in devices and characterization methods, both a result of improved processing technique, have lead to better understanding of science at the nano-scale thus improving simulation techniques. The idea is presented as a flow in Figure 1.

One of the limitations in present day electronic circuits is the interconnect technology. By the year 2010 it is expected that IC chips will comprise 10^9 transistors with 4nm thick gate oxides and 100nm minimum feature size running at 4GHz clock speeds [9]. It is conceivable that incremental advances in chip architecture will compliment improvements in materials and fabrication technology. However, signal propagation delay (between transistors) is still larger than device gate delay (delay within device).

Resistance and capacitance associated with fine line aluminum and copper interconnects, traditionally used in chips, limits speed and increases power consumption and crosstalk. Principal issue is the RC gate delay in electronic interconnects.

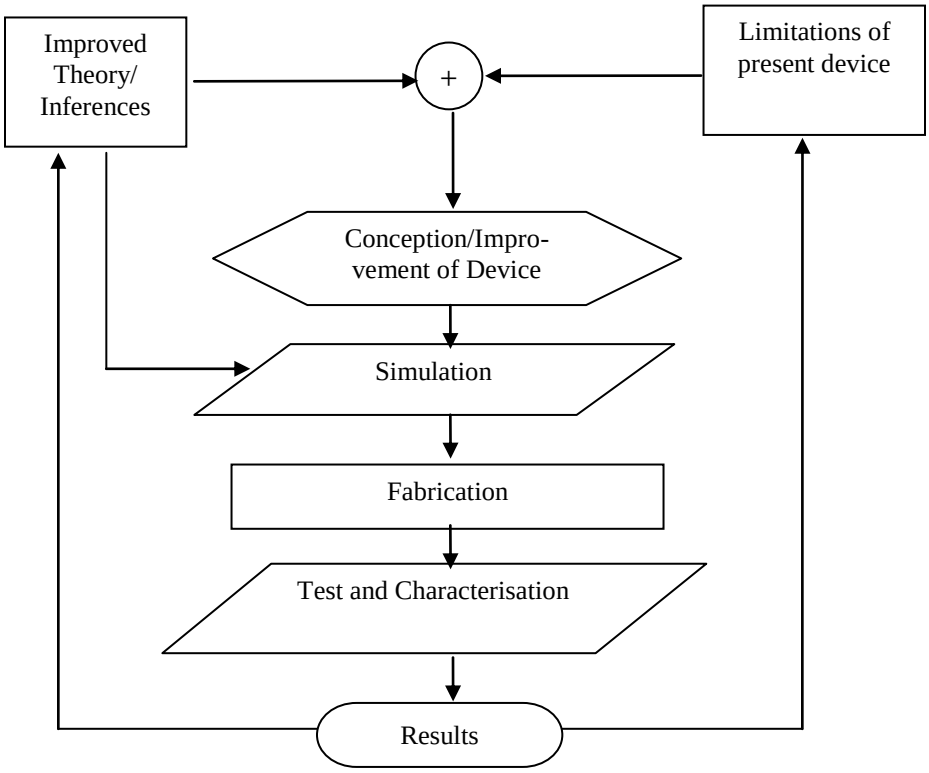

Figure 1: Positive feedback favoring micro and nanotechnology.

If we assume resistance (R), capacitance (C), area (A), length (l), thickness (d), ρ as density and $\in$ as the permittivity then -

$$R = \rho \cdot \frac{l}{A}$$

and the capacitance is

$$C = A\frac{\in}{d}$$

time constant 'τ' ($\tau = R \cdot C$) is thus

$$\tau = \rho \cdot l \cdot \frac{\in}{d}$$

Transmission delay is independent of interconnect cross-section area. Although reducing device dimensions increases computational complexity within the same area but signal transmission delay remains the same. Optical interconnection can remove electronic transmission bandwidth limit. An optical waveguide with strong light confinement allows dense and sophisticated optical wiring in photonic integrated circuits (PICs) [10].

Revolutionary replacement of copper cables in transmission lines with optical fiber backbone transmitting data between continents at enormous speeds is the fundamental enabler of World Wide Web. Analogically, nano-sized optical interconnects could be used instead of copper lines for their potential advantages over metal in semiconductor chips. The challenge is development of silicon IC compatible micro-photonic technology. Additionally if the chosen material is silicon then incorporation of these optical devices with CMOS circuits simplifies further, relatively. Silicon photonics maybe defined as design and fabrication of photonic devices using traditional Si-CMOS techniques in addition to providing substantial size, cost, and power savings, the integration of optics technology to the present electronic-only circuits.

1.1. Absorption

Silicon absorbs light in a different band of electromagnetic energy than the communication wavelength[*]. If the energy of the incident photon is less than the band

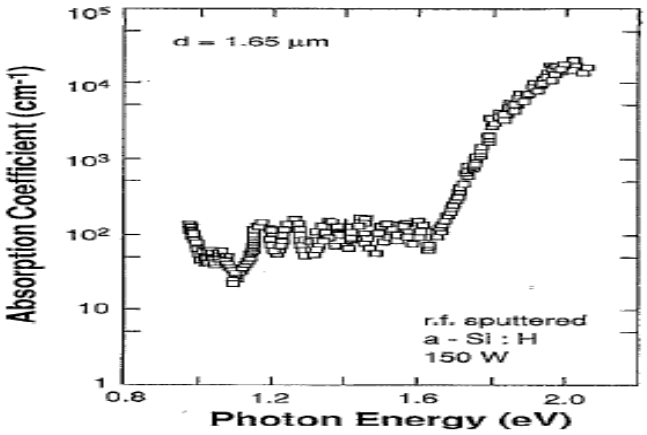

Figure 2: Absorption spectrum of amorphous silicon film of thickness 1.65µm varying by two orders of magnitude between incident photon energies of 1.6 to 2eV.

The behavior of amorphous silicon as a photo transducer for high-energy photons and transparent media for low energy photons is aptly described by plot shown in Figure 2.

1.2. Refractive Index

[*] This wavelength is specified by the fiber being deployed in WAN (wide area networks) or MAP (metropolitan area networks). It is usually around the so called communication wavelength of 1550nm.

Another property of silicon, which is instrumental in its choice as optical interconnects, is high refractive index compared to silica (SiO_2). As shown in Figure 3, for low photon energies refractive index is higher than 3.

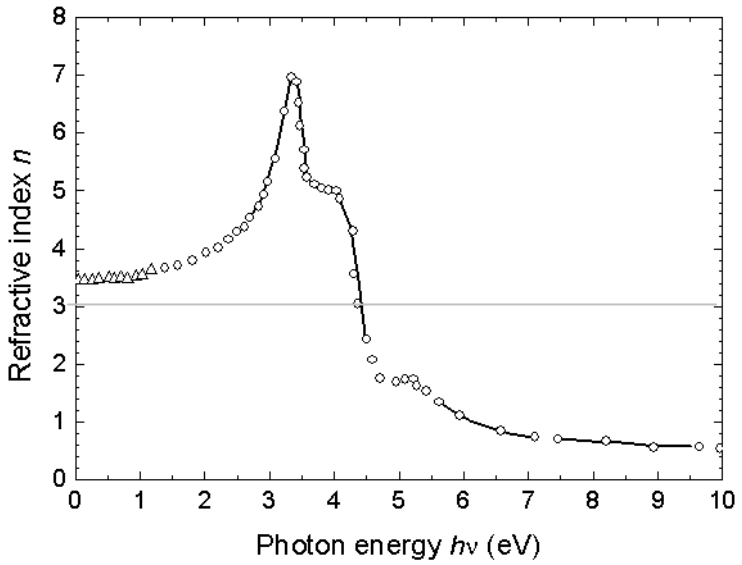

Figure 3: Refractive index of silicon as function of photon energy.

Introspection

Irrespective of choice of technology in electrical interconnects the minimum delay per unit length is the same and cannot be reduced any further, Figure 4. Signal propagation delay is thus a bottleneck in the electrical domain as device gate delay is smaller than signal propagation delay in presently employed interconnects. For faster operation alternatives are needed. Figure 5 shows standard deviation in delay in electrical and optical domains with decreasing interconnect dimensions and increasing time, the results compare favorably for optics.

In optics though, miniaturization (contrary to electronics which have flourished for their scaling prowess) of optical interconnects is a significant concern. To be able to replace the metallic interconnects, thousands of optical interconnects are required per chip!

1.3. Waveguides

Different structures may be used to fabricate optical waveguides. Simplest among them is the slab waveguide, which has a uniform high-refractive index layer on a low-index cladding layer.

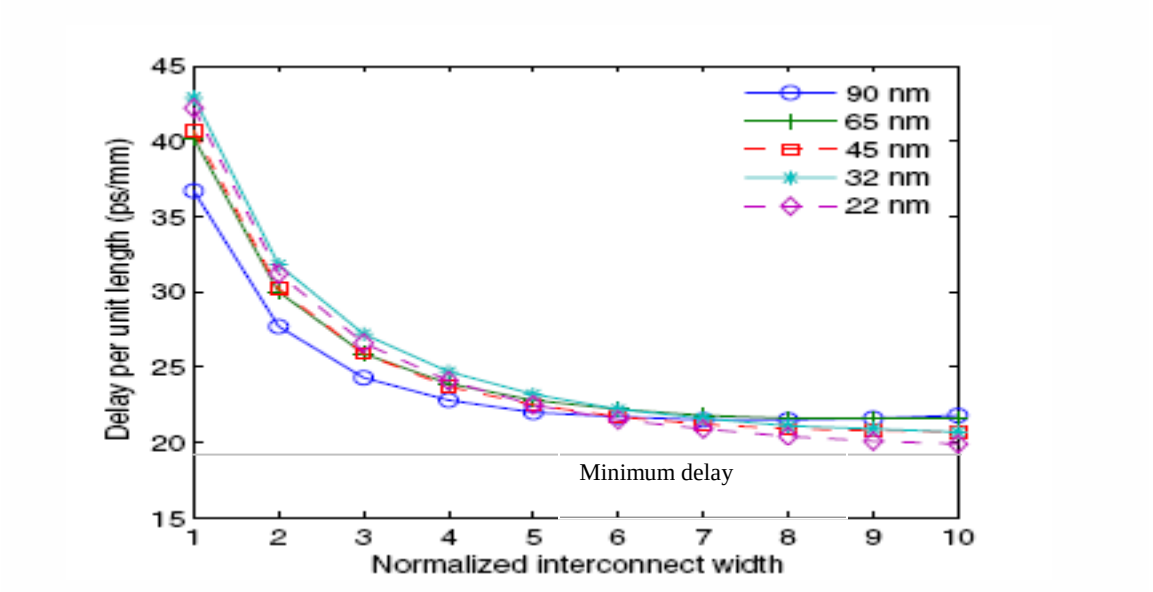

Figure 4: Minimum delay per unit length as a function of interconnects width in the electrical domain [26].

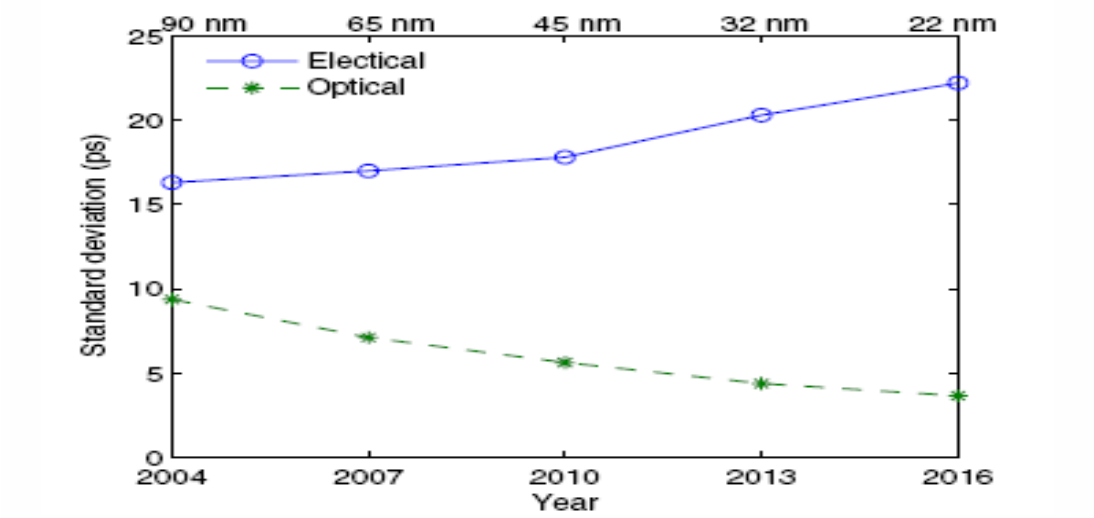

Figure 5: Comparison of standard deviation of delays in electrical and optical interconnects [26].

Slab waveguide (Figure 6a) offers only lateral confinement, and cannot therefore confine light horizontally. Transverse confinement may be achieved by various structures. A strip waveguide (Figure 6b) can be formed from the slab structure with photolithography and etching techniques. After etching of the waveguide structure, a top cladding layer may be deposited to provide a uniform low-index surrounding the core. Similar procedure is

followed for rib waveguide (Figure 6c) except that the high-index core layer is not fully etched. However, the difference between the effective indexes of partially etched slab and rib is sufficient to confine light within the rib section. In strip-loaded waveguide (Figure 6d), a strip of lower refractive index is deposited on top of a slab waveguide, resulting in a guided electromagnetic (EM) wave just below the strip. Diffused waveguide (Figure 6e) is achieved by local doping with an element, which increases refractive index of the core with respect to the cladding.

Scheme for subsequent figures-

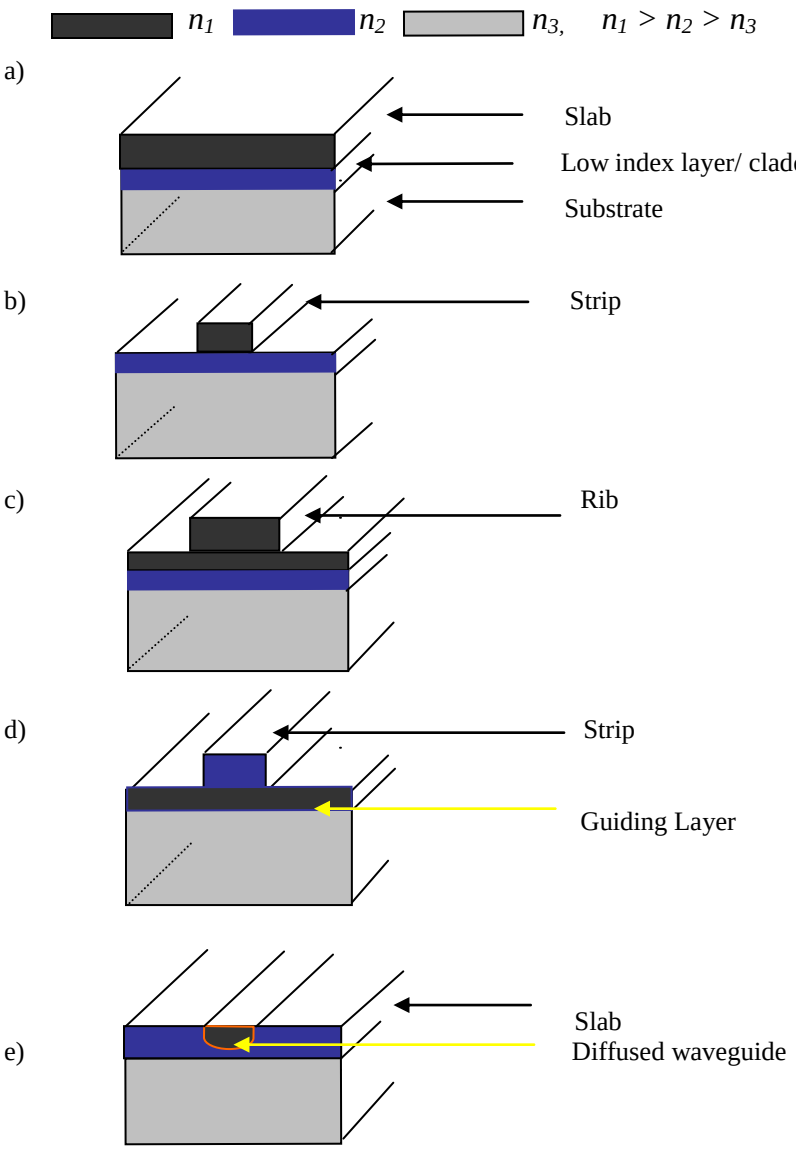

Figure 6: Different waveguide structures are shown in the figure: a) Slab, b) Strip, c) Rib, d) Strip Loaded, e) Diffused.

Analogous to electrical circuits where electrons flow from higher to lower potentials, light has an affinity towards areas of higher refractive index.

1.4. Different Waveguide Materials and Properties

III-V Semiconductors

These are compounds belonging to the group three and five of the periodic table of elements. The photonic devices which are fabricated by deposition and micro-machining of these compounds produce low losses, and so far, are the only sources of producing lasers and other active devices which are essential for integrated photonics [25].

Figure 7 shows 'transmitter' side of the communication system. It has a laser actuated by electrical pulses sensed by a detector. Detector could also be a modulator varying the output of the laser by some other actuation mechanism. The laser light via optical interconnects is transmitted to the modulators where light is suitably modulated and sent for transmission through single mode fibers.

$LiNbO_3$

Lithium niobate is another prospective compound used to form waveguides and the process involved is titanium diffusion or proton exchange. Losses as low as 0.1dB/cm have been reported.

Figure 8 depicts the flow of the fabrication process. On lithium niobate (substrate) photoresist is deposited by spin coating. The photoresist is then patterned by optical lithography. Next step is titanium deposition by sputtering. Titanium deposits uniformly over the whole surface.

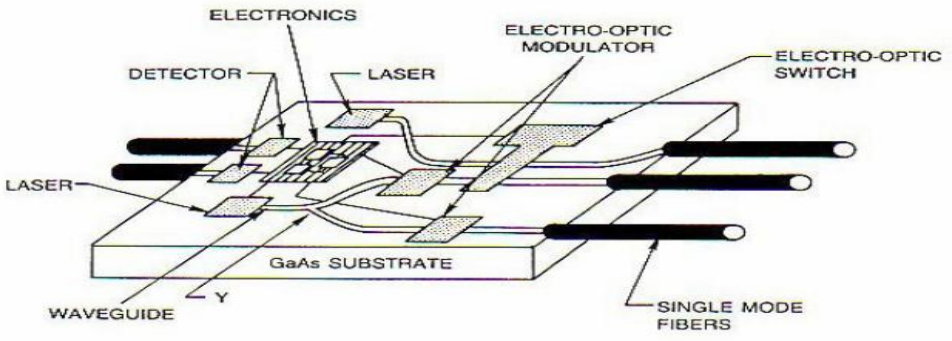

Figure 7: Demonstrative layout of an integrated III-V compound hybrid device [38].

Lift off is then performed, the substrate is dipped in a solution of acetone and metal above the photoresist is dissolved along with photoresist. Thus a substrate with patterned titanium is obtained. It is then placed in the furnace at high temperatures (1000˚C) where thermal diffusion of titanium into lithium niobate substrate occurs. Suitably varying the furnace temperatures or using spacers can also tailor the profile of buried waveguide.

Silica on Silicon

Step index waveguides with symmetric rectangular cross-section are formed. A thick SiO_2 layer covers silicon substrate and then doped SiO_2 is deposited as the core. Using photolithography the core is patterned and then another layer of SiO_2 is deposited. The processing steps are shown in Figure 9.

The grey layer is silicon substrate, on which SiO_2 is deposited. On top of this layer doped SiO_2 is deposited (dark blue). This layer is then patterned by lithography and etching. Finally conformal deposition of another layer of SiO_2 is carried out. The process yields a high refractive index core of SiO_2 on top of Si and over cladding is undoped SiO_2.

Ion Exchanged Glass Waveguides

These waveguides have demonstrated minimum losses but their compatibility with other III-V compounds and integration with CMOS fabrication techniques is difficult. They also show low birefringence. The fabrication process is demonstrated in Figure 10 below.

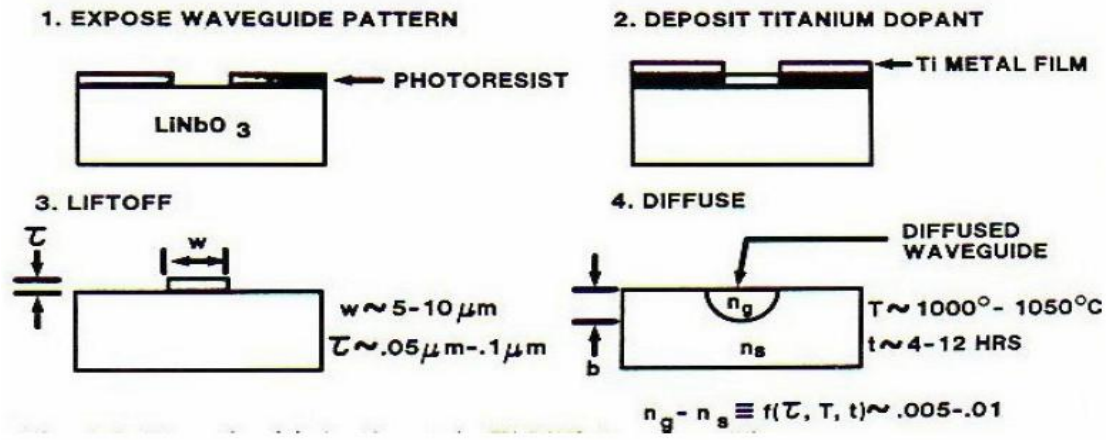

Figure 8: Schematic of the fabrication process in $LiNbO_3$ substrate using titanium diffusion by thermal annealing [29].

Firstly titanium, or other mask material, is deposited and patterned by lithography and etching. Substrate is dipped in a concentrated solution of silver ions. At this stage ion-exchange occurs. Titanium mask is then removed. Finally electric field is used to bury the ion exchanged silver ions deeper, yielding a buried waveguide.

Polymer Waveguides

LAN and cabinet-to-cabinet optical interconnects are needed today in enterprise environments, for entertainment and control systems in the 'Digital Home', and for intra-vehicular communications in the automotive and aerospace industries. Polymer optical fiber (POF) is used for these short reach data link applications that require simplicity and low cost. The only hurdle in their widespread use is reliability. For similar advantages of robustness and tunable chemical-mechanical properties polymeric waveguides are now used in mobile phones and display panels for illumination purposes. The polymeric waveguides are susceptible to atmospheric conditions and require careful packaging and encapsulation (unlike crystalline, polysilicon (poly-Si) and amorphous silicon which are hard and can work well with an inert cladding of SiO_2). Losses as low as 0.01dB/cm have been reported and polymer materials are ideally suited for sharp bends and nanoscale structures. Use of imprint lithography may also tilt the balance in favor of polymeric waveguides. These interconnects have already been demonstrated on circuit boards as shown in Figure 11.

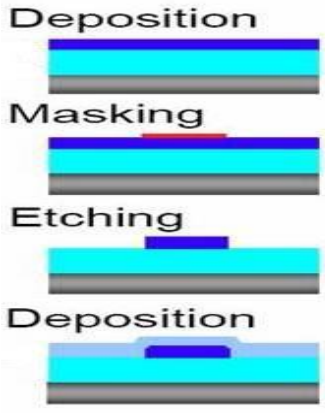

Figure 9: Schematic of fabrication of silica on silicon waveguides [29].

In the following report Chapter 2, *Theory* lays the groundwork for measurements and analysis techniques that are presented in Chapter 3, *Measurements*. In Chapter 4 SOI

devices are studied. Shortcomings and means to improve the presented research are discussed in Chapter 5. Chapter 6 concludes the study with suggestions for future work. An international conference paper is published based on the findings; its details are summarized in *Publication*.

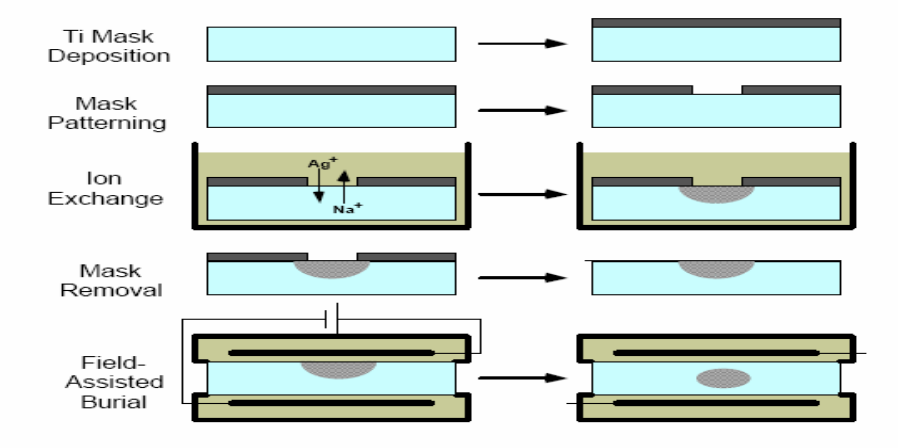

Figure 10: Field assisted burial of Ag in glass waveguides by ion exchange [29].

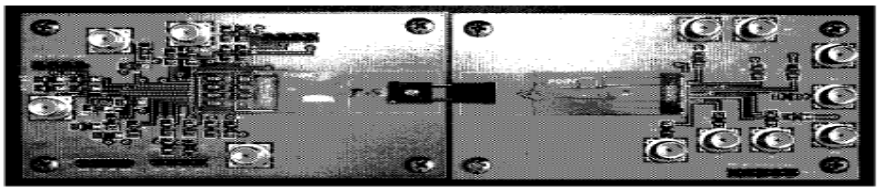

Figure 11: Polymeric interconnects on a PCB.

2. Theory

In this section various aspects of optical waveguides – material, geometrical, mathematical and clean room processing.

2.1. Ray Optical Model

Let us consider a slab waveguide structure (Figure 6a) where n_1, n_2 and n_0 are the refractive indices of slab, substrate and air, respectively, and '$2a$' is the height of the core.

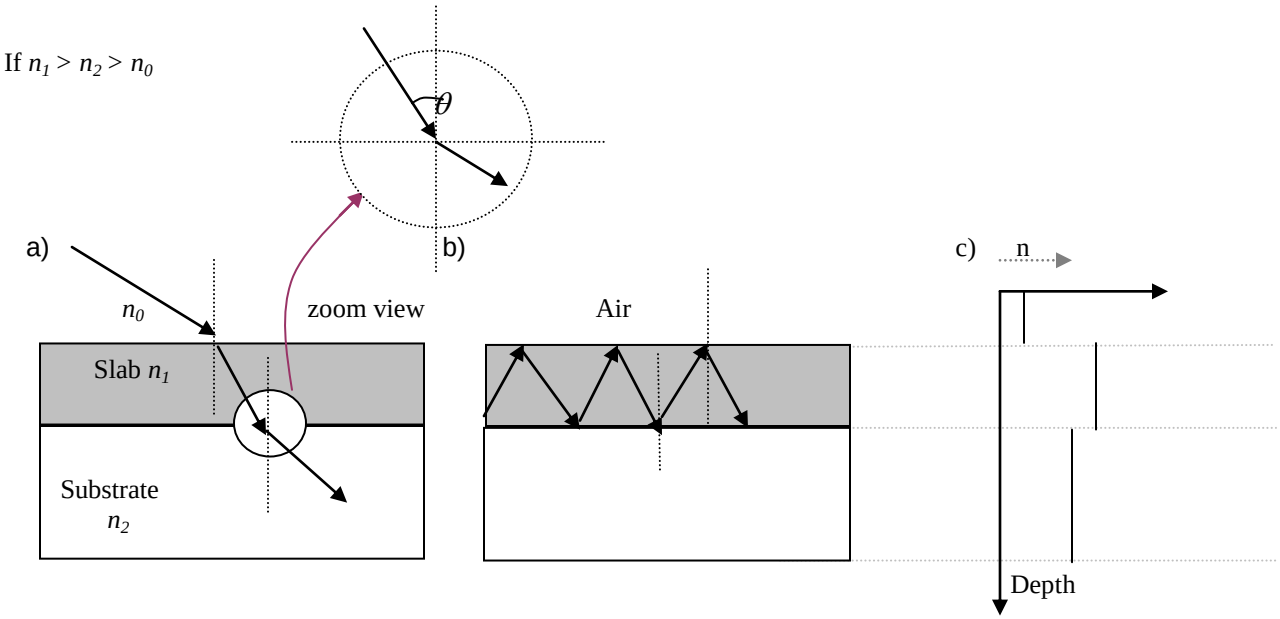

Figure 12: a) Three media refraction model, zoomed at n_1-n_2 interface, b) guided wave propagating as zigzag ray obeying Snell's law, c) plot of refractive index vs. height of the structure.

If '$\theta > \sin^{-1} n_2/n_1$' then total internal reflection will occur as shown in Figure 12b (Snell's law). Consider two rays originating from same wavefront (Figure 13), which satisfy the condition for total internal reflection, to enter the slab. Ray 1 undergoes two reflections at *A* and *B* and is traveling parallel to Ray 2. Unless wavefront of Ray 1 just after reflection at *B* is in phase with wavefront of Ray 2 at *B*', these two rays will interfere destructively. Change in phase between Ray 1 and Ray 2 due to path difference is K_1 *(AB - A'B'),* where '$K_1 = 2\pi n_1/\lambda$', is the propagation constant.

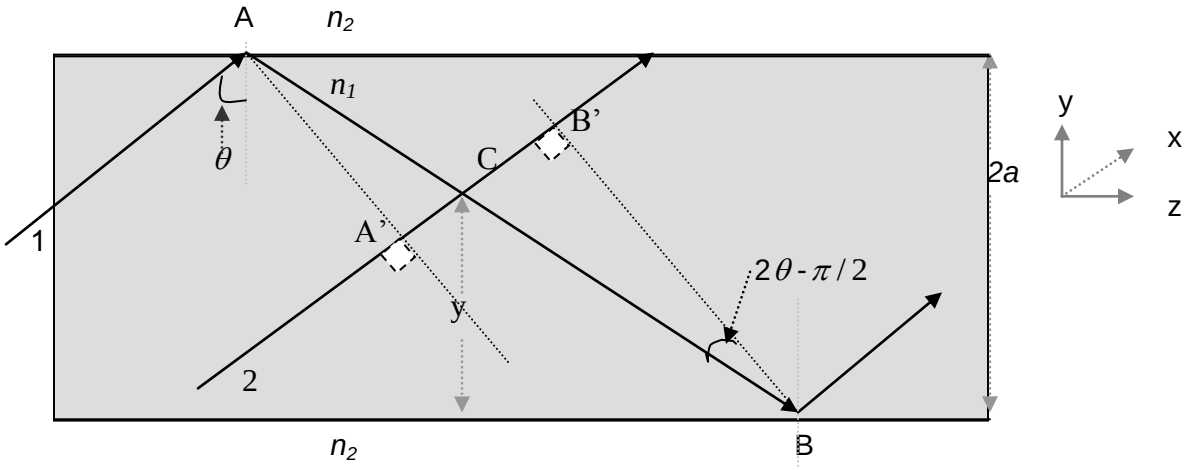

Figure 13: Ray model for illustrating phase matching conditions and interference within the waveguide.

Let phase difference due to reflection at points *A* and *B* (media interface), each equal ϕ_m.

Then cumulative phase difference between the two rays must be equal to $2m\pi$ for constructive interference, which gives the following condition,

$$K_1(2a)\cos\theta - \phi_m = m\pi \quad \text{---(1)}$$

This simplistic analysis shows that only a discrete set of θ are allowed within the waveguide corresponding to integral values of *m* for a wavefront to propagate successfully. Resolving wave vector K_1 into *y* and *z* axes as β and κ respectively*,

$$\beta_m = K_1 \sin\theta_m = \frac{2\pi n_1}{\lambda}\sin\theta_m$$
$$\kappa_m = K_1 \cos\theta_m = \frac{2\pi n_1}{\lambda}\cos\theta_m \quad \text{---(2, 3)}$$

Further, for these discrete modes (corresponding to θ) that can travel, mathematical analysis shows there is a stationary electric field pattern along *y* axis traveling towards *z* direction with a propagation constant β_m. Consider resultant of multiple rays at an arbitrary point within the slab, for example *C*. Rays 1 and 2 meet at *C*. Effective phase difference between the waves when they meet at *C* is

$$(K_1 AC - \phi_m) - K_1 A'C = 2K_1(a - y)\cos\theta_m - \phi_m \quad \text{---(4)}$$

Simplifying; phase difference Φ_m is

* Notice the usage of *m* in the subscripts of β and κ corresponding to different angles of incidence.

$$\Phi_m = m\pi - \frac{y}{a}(m\pi + \phi_m). \qquad \text{---(5)}$$

Thus, electric fields of Ray 1 and 2 before they meet at *C* are

$$\begin{aligned} E_1(y,z,t) &= E_0 \cos(\omega t - \beta_m z + \kappa_m y + \Phi_m) \\ E_2(y,z,t) &= E_0 \cos(\omega t - \beta_m z + \kappa_m y) \end{aligned} \quad . \qquad \text{---(6, 7)}$$

These two waves interfere to give

$$E(y,z,t) = 2E_0 \cos(\kappa_m y + \frac{1}{2}\Phi_m)\cos(\omega t - \beta_m z + \frac{1}{2}\Phi_m) \quad . \qquad \text{---(8)}$$

It may be observed (8) that amplitude is a function of *y* alone and not *t*, thus there is a standing wave along the waveguide[*]. This is a simplified model and takes into account confinement only in one dimension. Note also that upper and lower cladding surfaces are assumed to be of the same refractive index, which is seldom the case.

Using Snell's Law, '$\sin\theta_m > \sin\theta_c$' and the condition for constructive interference derived above (1), following is proved mathematically

$$m \le \frac{(2V - \phi)}{\pi} \quad , \qquad \text{---(9)}$$

where $V = \frac{2\pi a}{\lambda}(n_1^2 - n_2^2)^{\frac{1}{2}}$.

These relations (9) are derived in various optics text books [19].

2.2. Wave Optical Model

The Maxwell's equations may be written in a non-conductive, charge free, isotropic media as (10)

$$\begin{aligned} \nabla \times \vec{E} &= -\mu \frac{\partial \vec{H}}{\partial t} \\ \nabla \times \vec{H} &= \varepsilon \frac{\partial \vec{E}}{\partial t} \\ \nabla \bullet (\varepsilon \vec{E}) &= 0 \\ \nabla \bullet (\mu \vec{H}) &= 0 \end{aligned} \qquad \text{---(10)}$$

The vector quantities are electric field strength $\vec{E}(x,y,z,t)$ and magnetic field strength $\vec{H}(x,y,z,t)$. Using the following vector identity

[*] To observe shape of the wave at a specific instant perpendicular to the plane of propagation, substitute z=0 and t=0. Consequently, the 2nd cosine term becomes a constant.

$$\nabla \times \nabla \times E = \nabla(\nabla \bullet E) - \nabla^2 E \qquad \text{---(11)}$$

and considering the harmonic time dependence, e^{-jwt},

$$\nabla^2 \vec{E} + \omega^2 \varepsilon \mu \vec{E} = -\nabla\left(\vec{E}\frac{\nabla \varepsilon}{\varepsilon}\right), \qquad \text{---(12)}$$

where ∇^2 is the Laplacian operator defined as

$$\nabla^2 = \frac{\partial^2}{\partial x^2} + \frac{\partial^2}{\partial y^2} + \frac{\partial^2}{\partial z^2}. \qquad \text{---(13)}$$

Similarly for $\vec{H}$

$$\nabla^2 \vec{H} + \omega^2 \varepsilon \mu \vec{H} = -\frac{\nabla \varepsilon}{\varepsilon}(\nabla \bullet \vec{H}) \ . \qquad \text{---(14)}$$

If dielectric constant of slab and cladding are assumed to be constants ε_1 and ε_2 respectively, then the wave equations are

$$\begin{aligned} \nabla^2 \vec{E} + \omega^2 \varepsilon_i \mu \vec{E} &= 0 \\ \nabla^2 \vec{H} + \omega^2 \varepsilon_i \mu \vec{H} &= 0 \end{aligned} \ . \qquad \text{---(15, 16)}$$

Harmonic dependence in the propagation direction may be assumed as $e^{-j\beta z}$. Thus,

$$E = E(y)e^{j(\omega t - \beta z)}. \qquad \text{---(17)}$$

As above, this analysis is valid only for slab waveguide. Since confinement of light in x direction does not occur, dependence of electric field in that direction is ignored. Velocity of light is 'c/n' in a medium of refractive index n (=$\sqrt{\varepsilon}$). Substituting these conditions into the wave equation (Equation 15)

$$\frac{\partial^2 E(y)}{\partial y^2} + (k^2 n_i^2 - \beta^2)E(y) = 0 \ , \qquad \text{---(18)}$$

where $k = \frac{2\pi}{\lambda}$.

If all possible values of β are considered, a wide range of solutions can be found. A qualitative description of the complete set is presented below.

Case1: $\beta > k_0 n_1$ ---(19)

The solutions are exponential in all layers. Since this implies infinite field amplitudes at large distances from the guide, these solutions can be ignored.

Case2: $$n_2 k_0 \le \beta < n_1 k_0$$ **---(20)**

There are a discrete number of bound or guided modes. These vary cosinusoidally inside the guide core, and decay exponentially outside the guide.

Case3: $$|\beta| < n_2 k_0$$ **---(21)**

Solutions vary cosinusoidally in both the guide and substrate. Since these fully penetrate the substrate region, they are called substrate modes.

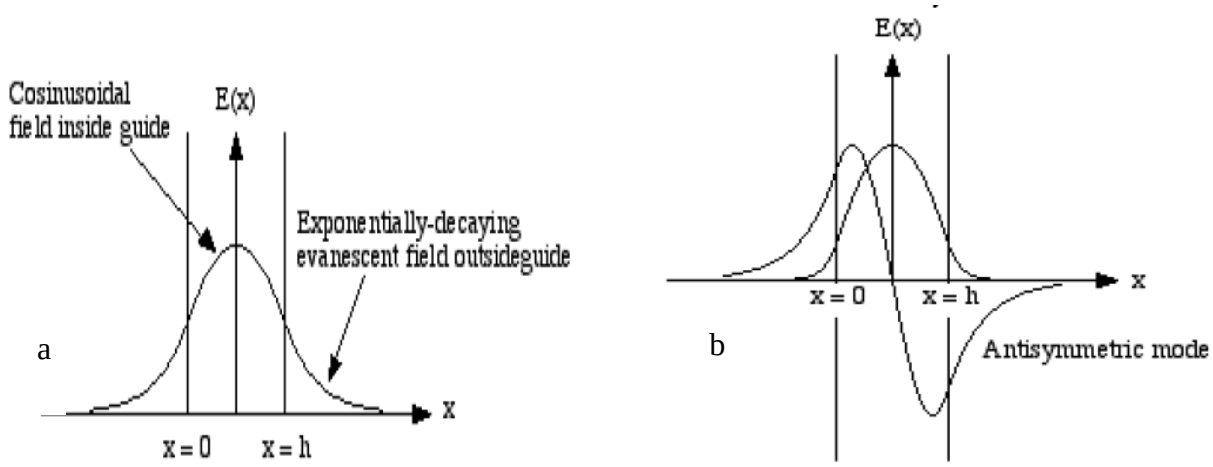

Figure 14a) Lowest order symmetric guided mode in a slab waveguide, b) Mode patterns of a two-mode slab waveguide [35].

The ray optical model and the analytical wave optical solutions for the slab waveguide are elementary demonstrative models and are not accurate to be used in modeling devices with 2-D confinement. The ray optical model does not take into account the wave nature of light and although it predicts the interference condition along with satisfactorily proving total internal reflection mechanism for guiding of light it fails to find cut off conditions for modes and their properties. The wave optical model, which uses the Maxwell equations, is able to provide satisfactory explanation for the modes and their effective index of refraction. For modeling 3-D waveguides various software tools are available commercially. Photon design Ver.4.3.1 is used for the simulations in this project.

2.3. Characteristics of Amorphous Silicon

In fabrication of optical devices various materials have been used for various devices. $LiNbO_3$ is used for high speed light modulators, GaAs for quantum dot exhibiting photoluminescence, InP for lasing applications etc. However, all of these materials are processed by techniques not compatible with the conventional CMOS processing line. The most commonly used equipments are metal organic vapor phase epitaxy (MOVPE) or hydride vapor phase epitaxy (HVPE). The fabrication techniques for silicon are advanced and thus suitably lend to fabrication of any silicon photonic device.

Structure

Amorphous silicon (a-Si) is the non-crystalline allotropic form of silicon. Silicon is a four-fold coordinated atom that is normally tetrahedral bonded to four neighboring silicon atoms. Unlike crystalline silicon (c-Si) where the tetrahedral structure is continued over a large range, forming a well-ordered lattice (crystal), in a-Si this long-range order is not present and atoms form a continuous random network. Not all atoms within a-Si are four-fold coordinated. In polycrystalline silicon (poly-Si) the crystalline order is followed in short sections after which another crystal orientation maybe present. This short range single crystalline region in polycrystalline silicon is called grain and their edges are called grain boundaries. This difference leads to different physical and chemical properties and responses to reagents.

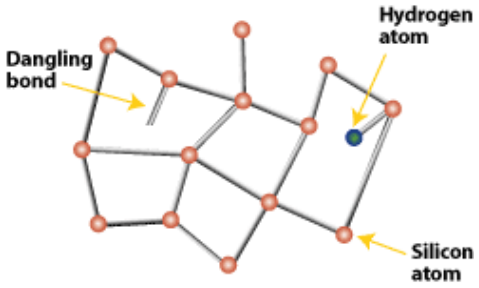

Figure 15: Random orientation of atoms in a-Si:H also illustrating association of dangling bonds to hydrogen atoms [36].

Polycrystalline silicon may be converted to crystalline silicon at 1200˚C. Similarly crystalline silicon may be converted to amorphous silicon by ion bombardment.

Fabrication and Processing

Amorphous silicon can be fabricated by PECVD, low pressure chemical vapor deposition (LPCVD) or CVD. In either case, the dangling bond density is high (Figure 15). These dangling bonds cause absorption and defects. To avoid them hydrogen passivation is carried out in PECVD. Moreover, a-Si:H may be deposited at low temperature of ≈120˚C (very low in the fabrication technologies). This feature of a-Si:H fabrication is very attractive since a-Si:H may be deposited on top of metals as well which have the strictest thermal budget in clean room fabrication technologies. Also, PECVD is a CMOS process and thus a-Si:H is compatible with the CMOS processing, one of its advantages that it shares with other allotropic forms of silicon. Etching of amorphous silicon is done by reactive ion etching (RIE). Smooth surfaces with root mean square (RMS) roughness of 0.3nm at the top of the waveguide and 0.5nm at the top of etched SiO_2 layer are detected by atomic force microscope (AFM), Figure 16.

Figure 16: Surface morphologies based on AFM measurements of a-Si:H waveguides deposited by PECVD at 250ºC.

Poly-Si is fabricated by LPCVD and the process temperature is ≈ 580˚C. Fabricated poly-Si may have void between the grains which would make them not suitable for waveguides. High thermal budget is required from components already deposited on the wafer. Etching in poly-Si can cause significant roughness on the side walls and this is the primary contributor to the losses that have been reported in polycrystalline waveguides [31].

Surface roughness produced via processing (deposition/etching) can be reduced by raising the fabrication temperatures during deposition or laser annealing after etching.

Crystalline silicon is grown e.g. by Czchochralski method where by a seed crystal is pulled out of the molten crucible. The seed crystal's structure is replicated on the growing and solidifying ingots. These ingots are then sliced to yield wafers of specific orientation. To grow single c-Si epitaxial growth has to be performed whereby the crystal orientation of deposited silicon is the same as the substrate silicon. This is a high temperature process and is very slow. Silicon on insulator (SOI) waveguides also exhibit low loss figures.

Etching is usually done by RIE and deep RIE (DRIE) enabling high aspect ratios with very low side wall roughness. Typically, surface roughness in c-Si can be as low as 0.2nm or even lower.

Absorption and Scattering

From the point of view of optical waveguides material absorption in waveguides is one of its fundamental characteristics. It is the lower limit of loss that maybe present in a passive element of the waveguide of that material. Lowest loss is present in c-Si; polycrystalline silicon and a-Si:H exhibits comparable losses depending upon the fabrication techniques. Value of loss reported in this thesis work is sum of scattering and absorption. In our sample of amorphous silicon the RMS value of roughness determined by AFM analysis is 0.6nm. The Tien's model (Equations 23-25) predicts the value of scattering loss to be around 12dB/cm. A satisfactory model for calculating scattering in more complex configurations is not present in scientific literature.

Refractive Index

The material refractive index determines how well light can be confined in it. Thus having a high refractive index number is decisive factor while deciding the right material for choice as a waveguide material. Figure 17 shows refractive index of a 260nm thick amorphous silicon layer on PECVD silicon oxide, measured by ellipsometry.

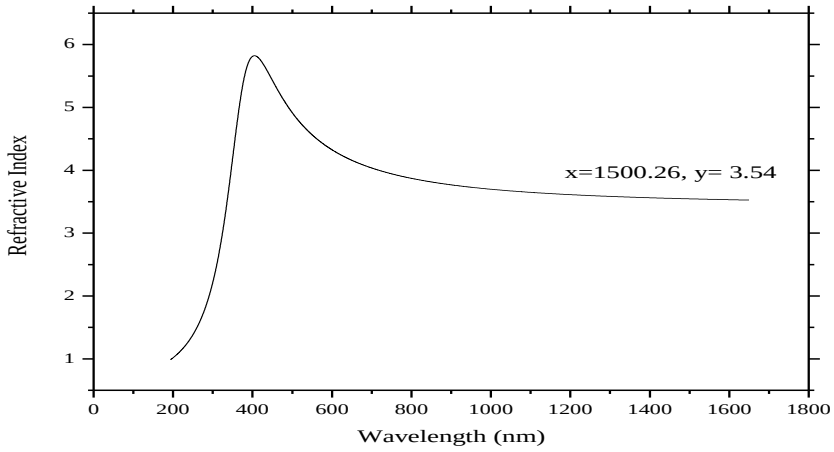

Figure 17: Refractive index of 260nm PECVD film of a-Si:H over thermally oxidized Si substrate.

Hydrogenated amorphous silicon exhibits good transparency between wavelength ranges 1.25-1.65µm. Refractive index can be calculated using the Cauchy's Law [12],

$$n = 3.2282 + \frac{0.2542}{\lambda^2} \qquad \textbf{---(22)}$$

In comparison, c-Si has a material index of 3.518 at 25˚C at 1550nm.

Defects

Due to disordered nature of the material in a-Si:H, some silicon atoms have a dangling bond. These dangling bonds are defects in the continuous random network, which cause high attenuation. The material can be passivated by hydrogen, which attaches to silicon atom and thus reduces dangling bond density by several orders of magnitude. Hydrogenated a-Si (a-Si: H) has sufficiently low amount of defects making it suitable for device applications [11].

By mid-90s interest in a-Si:H to be used at telecommunication wavelengths began to surge. It had previously been considered extensively because of high quantum efficiency in visible region of the spectrum [1]. Hydrogenated amorphous silicon has been considered for fabrication of optical waveguides due to two prominent factors. Firstly, processing needed to deposit a-Si:H does not require high temperatures. Procedures like PECVD can be used to deposit a-Si:H in 120-300°C range. This brings with it possibilities of deposition on almost any substrate, providing a high degree of versatility. Secondly, a-Si:H has a refractive index of 3.54[18], which offers good contrast with air and substrate materials.

Losses

One of the primary characteristics of an optical waveguide is its loss. There are two significant loss mechanisms within the waveguide, namely; scattering, and absorption. Other losses that are present in the waveguide are because of its functionality e.g. bending losses or coupling light between different parts of the device.

During absorption some energy of the electro-magnetic (EM) wave is converted to other forms, for e.g. thermal energy. Absorption is maximum when frequency of the EM wave matches with natural frequency of vibrations of electrons. Primarily, absorption occurs in c-Si for photon energies higher than the band gap energy but due to structural

randomness in a-Si:H, edge of the absorption band is not sharp. Energy may also be absorbed by various ionic impurities in the medium, which are polarized due to presence of EM wave, these ions couple to the electric field and oscillate.

Scattering of an EM wave implies that a portion of energy in the light beam is directed away from original direction of propagation. There are various kinds of processes contributing to scattering. Scattering is significant when the EM wave encounters an opaque molecule or particle, the size of which is equivalent to its wavelength. The molecule is polarized under the EM wave and oscillates with it. An oscillating particle becomes a source of radiation and light wave is isotropically radiated from it, which effectively means that some part of the incident radiation is re-radiated (generally the radiation pattern depends upon shape and polarizability of the molecule). This reduces the signal strength when phenomenon occurs for light propagating in the waveguide. Scattering due to particle with size comparable to the wavelength of radiation is called Rayleigh scattering.

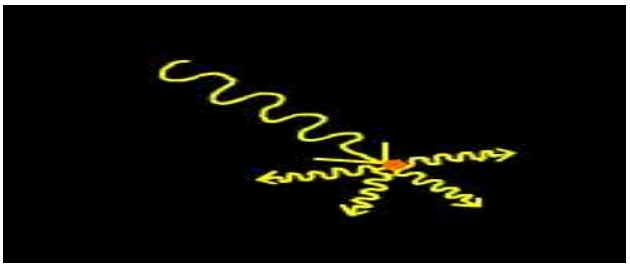

Figure 18: Small particle of the order of wavelength of light re-radiating the incident light beam isotropically [36].

Scattering may also occur due to surface roughness, briefly explained below. Contribution of losses due to surface roughness has been proposed by Tien [5]

$$\alpha = A^2 \left(\frac{\cos^3 \theta}{2 \sin \theta} \right) \left(\frac{1}{t_g + (\frac{1}{q}) + (\frac{1}{p})} \right)$$

$$A = \frac{4\pi}{\lambda} (\sigma_{21}^2 + \sigma_{12}^2) \quad . \qquad \text{---(23, 24)}$$

$$P(z) = P_o \exp(-\alpha z), \qquad \text{---(25)}$$

θ is the angle of rays propagating in the waveguide, *1/p* and *1/q* are penetration depths of the mode into the cladding (in the symmetric case, $p=q$), t_g is guide thickness and A is the measure of surface roughness where σ represents roughness of the interfaces at the top

and bottom of waveguides. In Equation 25, *P(z)* is power in the *z* direction and α is the attenuation constant. Tiens model proposed in 1971 has been widely used in scientific literature for predicting losses because of surface roughness. It is applicable for slab structures only and in the case of 2-D confinement it gives an unsatisfactory result since the loss predicted is higher than total loss measured in the waveguides.

Typically value of scattering is not very significant if the system has high absorption. If however absorption is less than 1dB/cm, then scattering is the most prominent contributor.

Coupling losses are generated due to mode field mismatch between fiber and waveguides. It could be significantly reduced if the light source is integrated on the chip. Single mode optical fiber has a core diameter of around 10µm and the multimode fiber has a core diameter of around 50µm. Coupling light from such sources to waveguides the dimensions of which are less than 5µm is difficult. Index matching oil has a refractive index of 1.5 and thus decreases reflections to the waveguide from the fiber core, which has a core refractive index of approximately 1.48. Light may also be collimated through a lens before coupling. Typical values of coupling losses are around 10-15dB in our experiments where no index matching oil or collimating lenses are used.

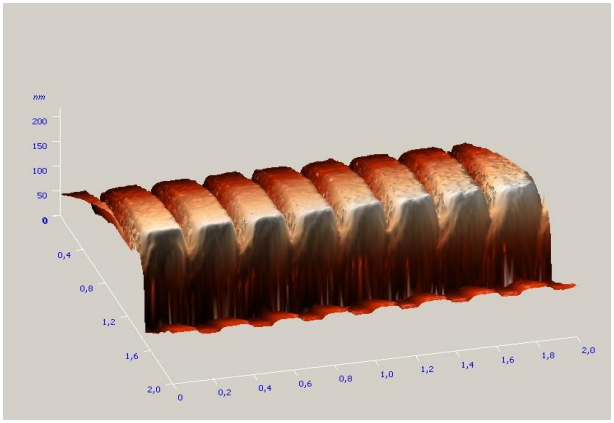

Figure 19: AFM picture of an a-Si:H strip waveguide with gratings. The surface roughness is low after hydrogen passivation. Scales of the three axes are in nanometers.

Losses due to reflection at the fiber joints, facets of the laser and detector, and polarizer are determined by measuring fiber-to-fiber losses. This value in our laboratory was statistically estimated to be 5-7dB. Scattering losses have not been measured in the waveguides. Observing the waveguide under the AFM suggested the surfaces are smooth.

Different methods are used to analyze different losses; a qualitative description of the procedures is presented below. The scattering losses can be estimated after finding the roughness of the structure by AFM. The functionality losses can be measured by measuring the loss in a straight waveguide without bends provided it is of the same length as the bent structure. This ensures all other parameters are kept constant. This must be ensured during the mask drawing and layout. For practical device purposes it is sufficient to remove the coupling and reflection losses from the observed data and safely assume rest to be a device parameter. Additionally, the smallest thickness of the slab of amorphous silicon that has been analyzed for its material parameters like refractive index and scattering is 10μm (*Fan et.al.*) which is way more than our thickness of 200nm, thus the refractive index has been characterized (Figure 17).

3. Hydrogenated a-Si Strip Waveguides

Interaction of light (EM waves) and matter is diverse. Analysis of this interaction may be exhaustively divided into two- "after light and matter interact if we investigate the medium we get information about the light and if we investigate light we are informed about the matter [17]".

In accordance with the above statement following measurements fall in the category where light (laser source) is investigated after its interplay with matter (a-Si:H strip waveguides). The aim of the measurements is to ascertain loss in the waveguides using two different techniques to ensure that there is consistency in results. In Cut Back method erbium doped fiber source (EDFS) is used as the source and in Fabry-Pérot method, a tunable laser source is employed.

Different research groups have used different measurement techniques [3-8]. Propagation loss of 40dB/cm have been reported in a-Si:H strip waveguides of height 0.25μm and width 0.5μm [14] and recently less than 1dB/cm in multimode rectangular waveguides and 2dB/cm in single mode ridge waveguides [37].

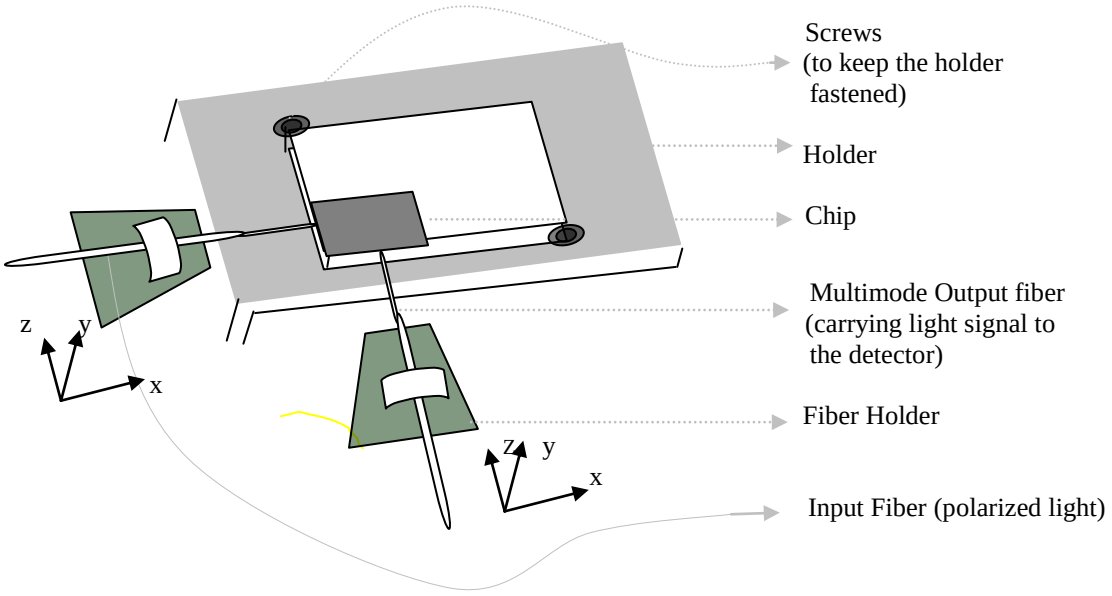

Figure 20: Alignment of optical fibers with the waveguides. Tri-axial alignment is possible with the optical fiber holder, in the direction of the axes shown.

The mask has bends ensuring that the measured light is from the waveguides and not the substrate. The input fiber is a polarization maintaining fiber. The fiber holders are fixed on *Milles Griot* mobile assemblies, with screws. These assemblies are used for tri-axial alignment of fibers to the chip. The sample (chip) is placed on the holder, which is fastened by screws on the bench. Input fiber transmits light from source, which could be an EDFA (Cut Back method), tunable laser (Fabry-Pérot method) or supercontinuum laser (spectral analysis) to the waveguides. Output multimode fiber is attached to the detector. The fibers are butt coupled to either end of the waveguide. For details of equipments used and their manufacturers refer Appendix I.

The Chip, W4C3

The under study Chip has been made on a 4" wafer of silicon. The wafer was thermally oxidized to grow SiO_2, then a-Si:H was deposited by PECVD. Photolithography using ultraviolet (UV) light and RIE was employed to pattern mask on the wafer. Mask used for fabricating waveguides on the chip was of size 2cm *X* 2cm. After fabrication the chip has four set of waveguides called series 1, 2, 3 and 4; with increasing length in that order. Each series has nine waveguides with width varying from 0.7 to 10µm. The waveguides are approximately 200nm in height and the spacing between them is either 50 or 100µm depending upon their width. Using the V-Number analysis (9), $m<2$, is obtained for the 200nm thick silicon slab. Thus, the waveguides are vertically single mode. Using a 1-D mode solver [16], effective refractive index, n_{eff} has been computed to be 2.73 for the TE_0 mode at λ = 1550nm.

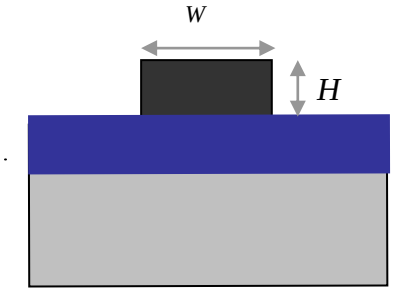

Figure 21: Profile view of a strip waveguide. Height *H* is 200nm and the width *W* has different values- 0.7, 1, 2, 3, 5, 6, 7, 8, 10µm.

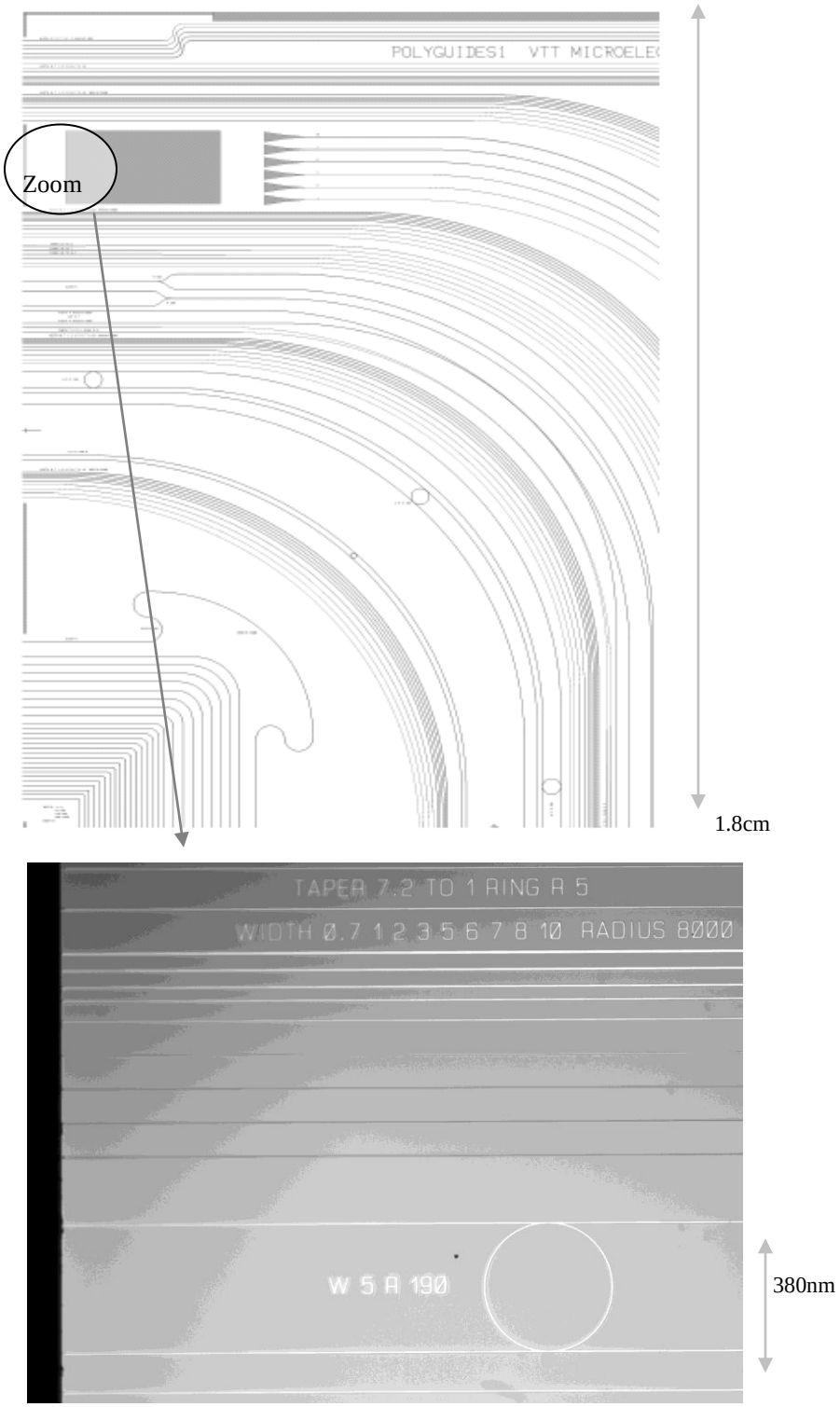

Figure 22: Mask used in lithography for fabrication above and the picture of the sample under an optical microscope.

3.1. Cut Back Method

Procedure

Input

The EDFA emits light in the wavelength range 1530 to 1600nm (Figure 25). Light from the EDFA propagates to the polarizer. From polarizer light is transmitted through the polarization sensitive fiber, other end of which is used to couple light into the waveguides on the silicon chip (Figure 20).

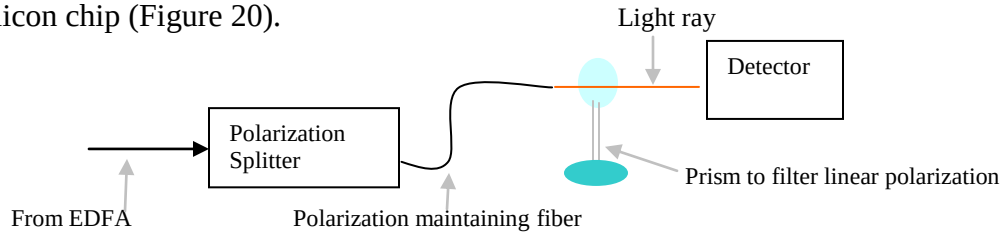

Figure 23: Schematic of the polarizer setup to check power in the TE and the TM modes.

Alignment

An optical lens system is used to check the fiber alignment to the waveguide facets. Similarly the output fiber (multimode) is aligned at the other end of waveguides (Figure 20). The multimode fiber feeds the InGaAs detector, where light is gathered. Also the power in the TE and the TM modes are compared to ascertain the proper functioning of the polarizer by the measurement setup shown in **Figure 23**.

Fiber-to-Fiber Losses

Both before and after finishing measurements fiber-to-fiber direct power is measured. Both input and output fibers are brought in proximity with their facets aligned so that highest power is sensed by the detector. Fiber-to-fiber reading acts as a reference between measurements done on different days since it represents inherent loss of the setup. This loss includes the loss in fiber connectors, reflection at junctions, polarizer and marginal power lost in the fibers.

Source Details

When excited, erbium ions return to their ground state, causing photoluminescence. The process of natural relaxation of ions from the excited state to the fundamental state

generates (emission of) non-stimulated photons with wavelengths spread over a wide spectral range.

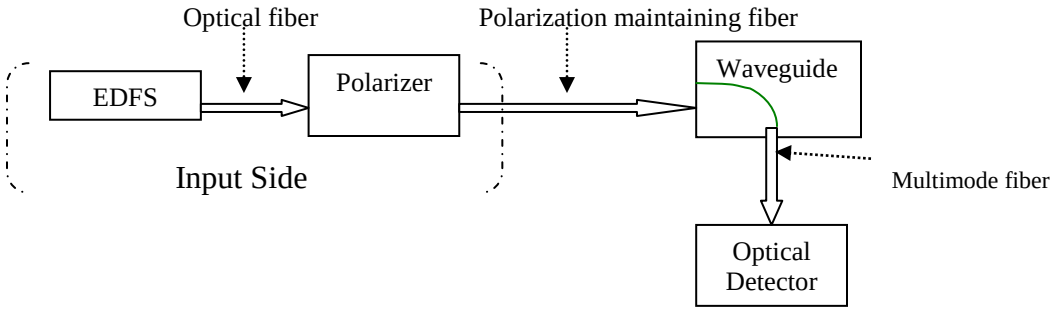

Figure 24: Schematic of the Cut Back method.

This is spontaneous emission noise (SE). However, since the EDFA is designed to amplify, the output signal is 'amplified spontaneous emission' or ASE. The aforementioned functioning of the device does not suitably lend it to be termed as an EDFA in our experimental method. It is more appropriate to term the device 'erbium doped fiber source' (EDFS). Illustratively, it is this amplified noise, the spectrum (Figure 25) of which is effectively input side of Figure 24.

Measurement Results

Fiber-to-Fiber power is -6dBm. Table 1 has different widths varying from 10 to 0.7μm. Values in the series columns are in dBm and represent detector power. The series 1 as shown in Table 2 has minimum length- progressively increasing towards series 4. Although shorter, series 1 shows higher losses than series 2 for some particular widths. This is on account of facet imperfections. The average value of each series (last row in Table 1) though shows, expected trend of, increasing losses with increasing length.

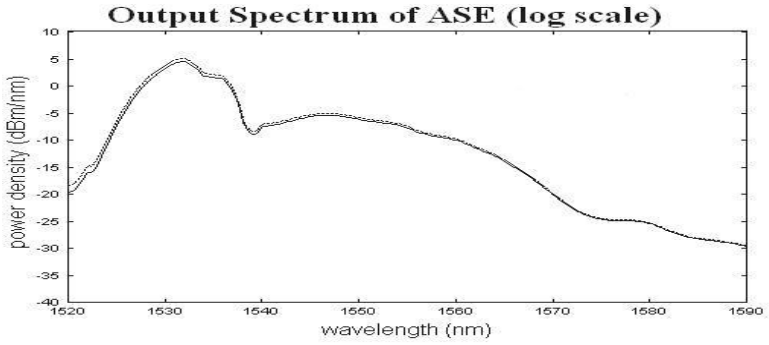

Figure 25: ASE spectrum of EDFA. The graph shows the wide spectrum of EDFS [34].

Width	Series 1	Series 2	Series 3	Series 4
10	-27.4	-28.3	-32.4	-42.8
8	-39.8	-28.2	-32.4	-37.6
7	-49.1	-30.7	-34.0	-34.4
6	-35.0	-31.7	-34.9	-38.8
5	-34.7	-31.8	-35.2	-35.4
3	-35.9	-35.3	-37.3	-39.4
2	-40.6	-43.6	-43.1	-47.2
1	-41.3	-64.8	-59.9	-65.2
0.7	-51.8	-66.0	-61.8	-67.7
Average	**-39.5**	**-40.0**	**-41.2**	**-45.4**

Table 1: Raw data from detector. Width is in microns, output power in the series is in dBm (last row-average values of each series). Unexpectedly, series 1 exhibits a higher loss than series 2 for various widths.

Series 1	1.10cm
Series 2	1.74cm
Series 3	2.39cm
Series 4	2.90cm

Table 2: Approximate length of different waveguide series.

Analysis by Cut Back method

This method statistically predicts loss due to coupling between fiber and the waveguide. Waveguides of specific width from different series are analyzed. Detected power is plotted against length. Linear regression (trend line) is done for each of these widths. Propagation loss is obtained from the slope of this line. To find out the coupling loss, the trend line is extrapolated to meet *y* axis. In theory this point is where waveguides are of zero length (x=0), thus reason for apparent loss (y coordinate) is coupling between the fiber and waveguide (Table 3).

Measurements depend significantly on alignment of the fibers to waveguide (Figure 20); one of the four lengths, which exhibited maximum variance from the trend line, has been excluded from final analysis (2.9cm in Figure 26). Using this procedure the 10μm wide waveguide has a coupling loss of 22dB and propagation loss, 3.89dB/cm (Figure 27).

Loss pattern in the waveguides of width 1 and 0.7µm was non conclusive (Table 1). Thus, these two waveguide widths are not included in the analysis*.

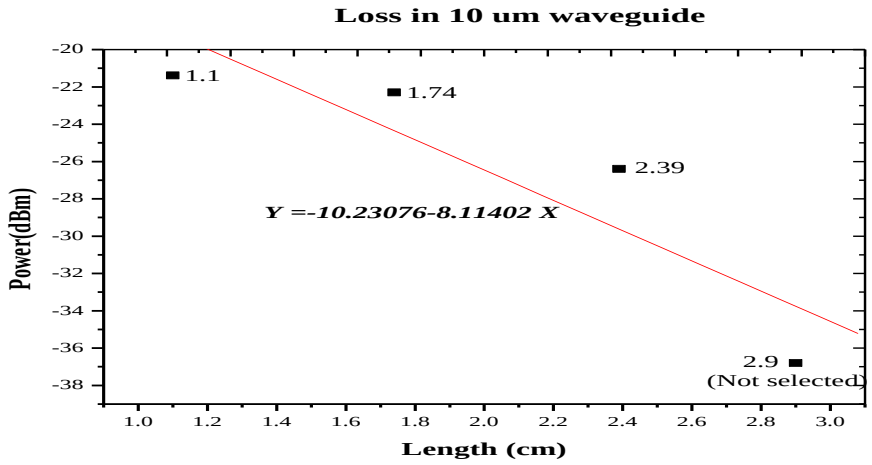

Figure 26: Loss for four lengths in 10µm wide waveguide. 2.9cm long waveguide shows maximum variance from the trend line and is omitted for cut back analysis.

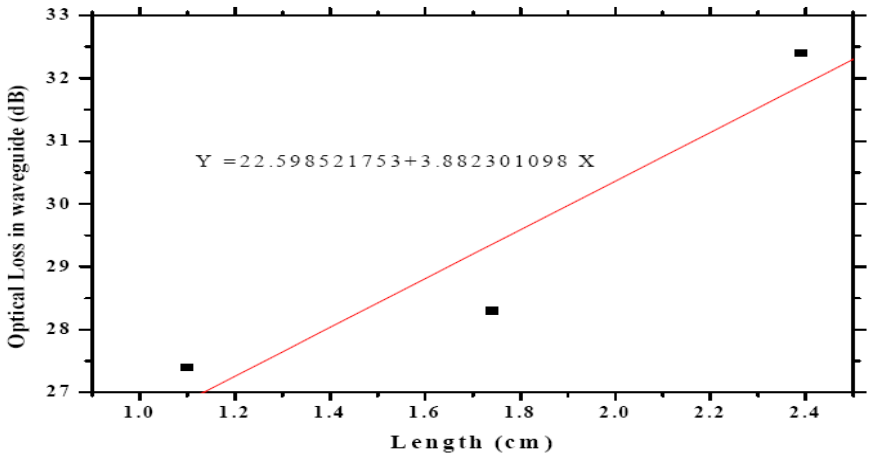

Figure 27: Plot for cut back analysis. From this curve, the coupling loss is 22.6dB (*y* intercept) and attenuation within the waveguide is 3.89dB/cm (slope).

Waveguides of width 6 and 8µm exhibit unusually high loss because their corresponding facets were inconsistent among different series. This may be attributed to the inclined facets, which cause inefficient coupling of light from fiber to the waveguides. It has been observed that keeping the fiber a little farther than closest to the waveguide edges results in better coupling of light. Most of the series 1 values exhibit maximum variance from

* However, even these two waveguides exhibited good sensitivity with respect to output fiber alignment. This proves that light, although feeble, is transmitted through them.

the trend lines; this may be observed in Table 1 where series 1 values are unexpectedly higher than series 2.

Width, μ m	'α', Loss in dB/cm	Coupling loss, dB
10	3.89	-22.6
8	8.03	-7.92
7	3.27	-19.36
6	6.07	-14.92
5	3.21	-20.64
3	3.52	-23.10
2	3.34	-30.51
1, 0.7	ND	ND

Table 3: Coefficient of attenuation and coupling power corresponding to different waveguide widths, ND: non determinable.

Error analysis by R squared (R^2) value: R-Squared is a statistical term informing how good one term is at predicting another. If R^2 is 1.0 then given the value of one term, you can perfectly predict the value of another term. If it is 0, then knowing one term doesn't help know the other term at all.

In Figure 27 the value of R^2 is 0.945, which is a good figure for reproducibility.

3.2. Fabry-Pérot Method

Procedure

Polarization is optimized using a polarizer plate and *FotecM* detector (**Figure 23**). Fiber-to-Fiber power loss is noted and TE mode has been considered for the measurements. The TE and the TM modes* have a difference of about 10dB in output power. Waveguide transmission is measured over the wavelength range 1550 to 1552nm (width=2nm) with a step size of 1pm and power 1mW. Labview is used to interface the detector and tunable laser with a computer. The scan can be performed with a step size of 1pm, 5pm or 10pm, over the wavelength range 1530 to 1630nm.

*TE mode is chosen mainly because it is better confined to the waveguide due to larger n_{eff}.

Source details

Tunable laser operates in the range 1520-1640nm, the emission is polarized, and 1mW power is used.

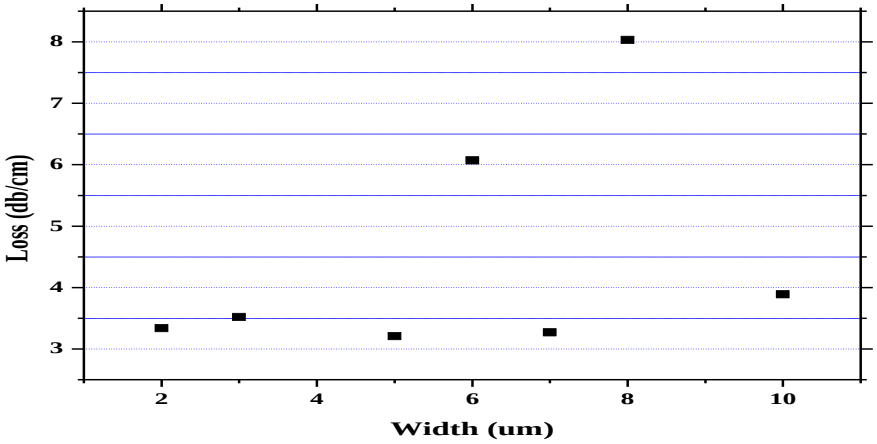

Figure 28: Loss with different waveguide widths. Most waveguides show loss between 3-4dB/cm.

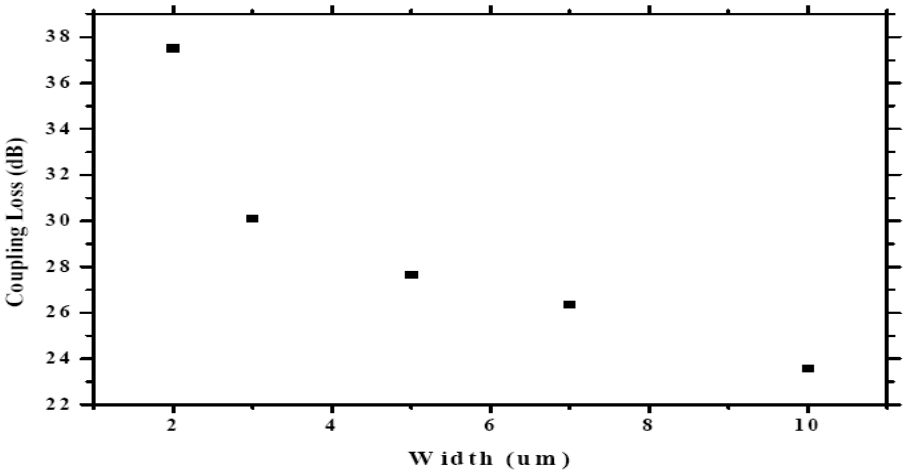

Figure 29: Coupling power loss vs. waveguide width. Coupling loss decreases as the width of the waveguide increases; this behavior is intuitive as more light would couple to wider waveguide. Single mode fiber, used for coupling light into the waveguides has a core diameter of 10-12µm.

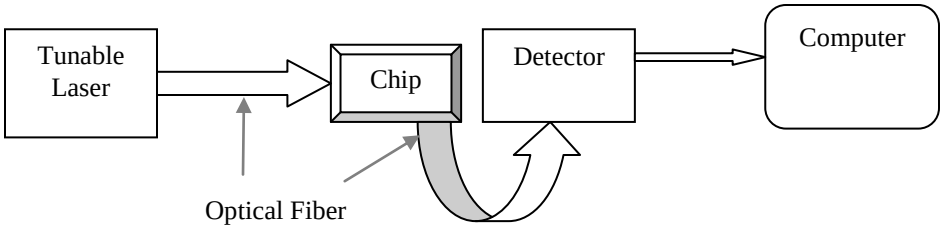

Figure 30: Schematic of the Fabry-Pérot method.

Measurement Results

Above spectrum (Figure 31) is zoomed-in to observe maximum oscillations, irrespective of the wavelength. However, without loss of generality, around the wavelength 1551.7nm a region of consistent oscillations is observed.

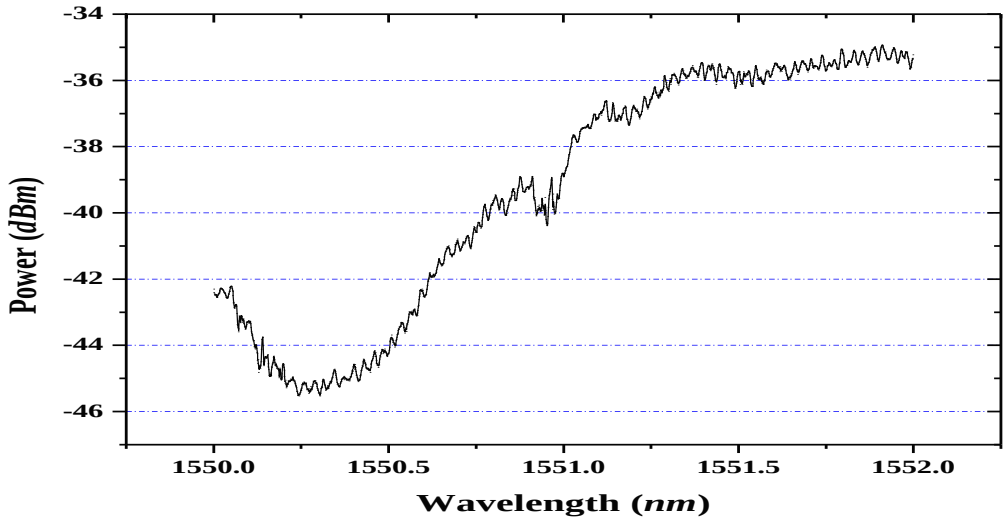

Figure 31: Graph shows the complete spectrum for Width =10µm, L=1.74cm.

For different widths the plots are shown hence, in Figure 32-35 low frequency components are removed and the spectrum is used to compute the amplitude of oscillations (Table 4).

Wavelength dependence of a Fabry-Pérot cavity transmission can be described as an Airy-function as follows

$$T(\lambda) = \frac{t_1^2 t_2^2}{1 + r_1^2 r_2^2 e^{-4\alpha L} + 2 r_1 r_2 e^{-2\alpha L} \cos\left(\frac{4\pi n_g L}{\lambda} + \phi_1 + \phi_2\right)} \quad \text{[31]. ---(26)}$$

Where L is the length of the cavity t_1, t_2, r_1 and r_2 are transmissivity and reflectivity of the mirrors. ϕ_1, ϕ_2 are the phase shifts generated by the mirrors, n_g is group index of mode propagating in the waveguide.

The phase shifts vary slowly thus not influencing the period in Equation 26. Thus we may assume,

$$\phi_1 + \phi_2 = 2\pi \ . \qquad \text{---(27)}$$

If all parameters in Equation 26 are wavelength independent then the following may be concluded $$\frac{1}{T(\lambda)} \propto 2A\cos\left(\frac{4\pi n_g L}{\lambda}\right). \quad \text{---(28)}$$

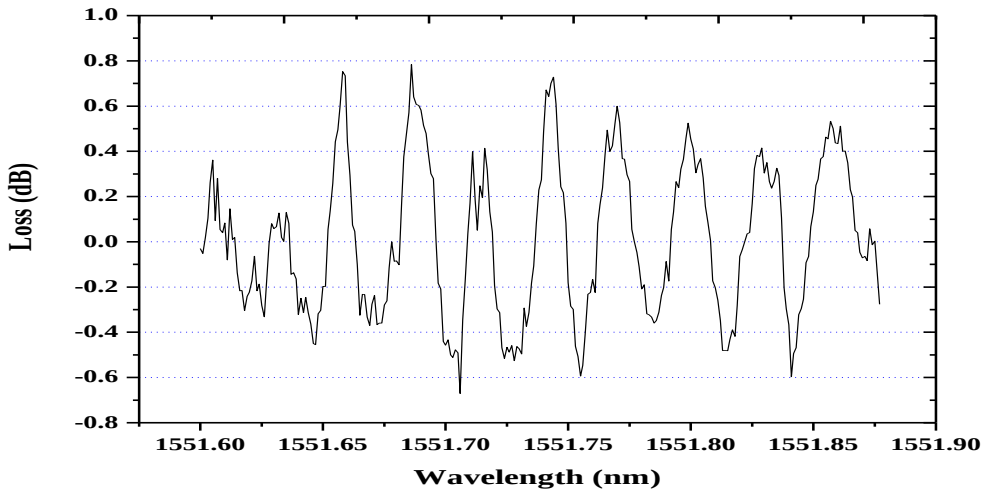

Figure 32: W=10µm, L=1.1cm, zoomed at 1551.756nm.

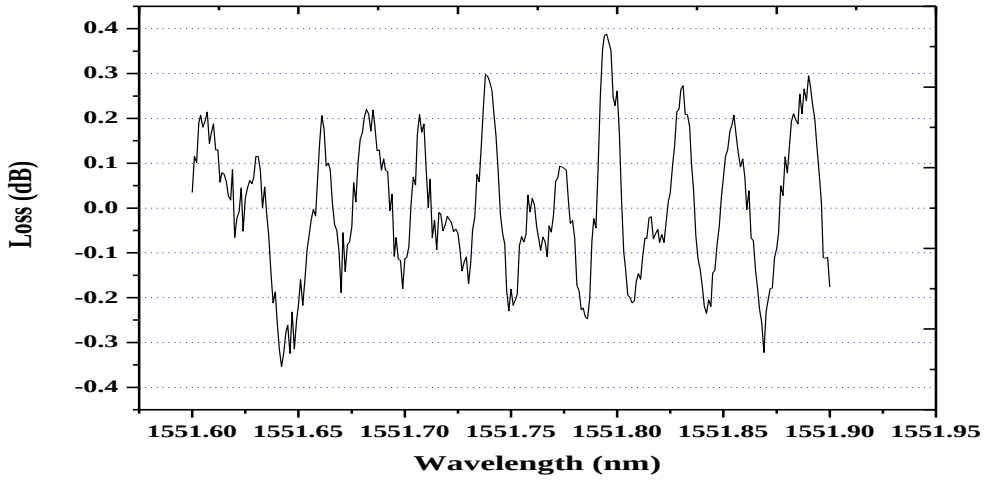

Figure 33: W=10µm, L=1.74cm, zoomed at 1551.79nm.

Dependence of 'T' on wavelength may be interpreted as oscillatory (Equation 28). Half amplitude of oscillation 'A' is determined by

$$A = r_1 r_2 e^{-2\alpha L} \quad , \quad \text{---(29)}$$

where ‘A’ is the fraction of electric field conserved after one round trip in the cavity. ‘A’ can be defined as the ratio between T_R and T_A; which are the transmission at resonance and anti-resonance.

$$T_R = \frac{t_1^2 t_2^2}{1 + r_1^2 r_2^2 e^{-4\alpha L} - 2 r_1 r_2 e^{-2\alpha L}} = \frac{t_1^2 t_2^2}{(1-A)^2} \quad \text{---(30)}$$

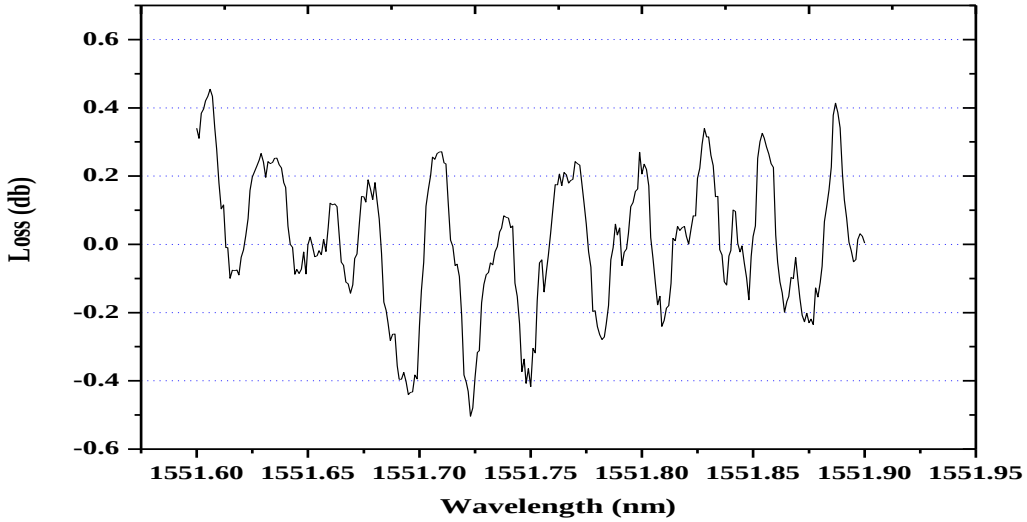

Figure 34: W=10µm, L=2.34cm, zoomed at 1551.708nm.

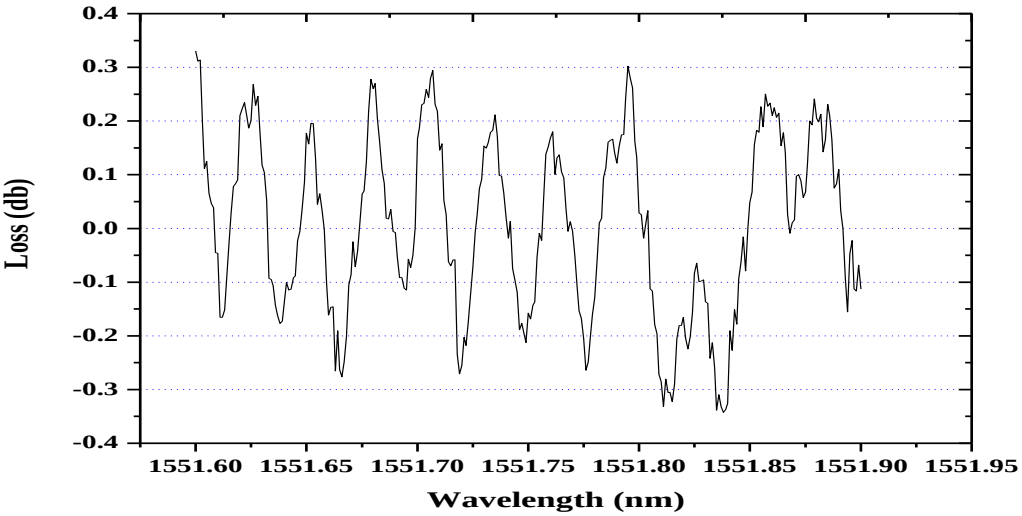

Figure 35: W=10µm, L=2.9cm, zoomed at 1551.79nm.

$$T_A = \frac{t_1^2 t_2^2}{1 + r_1^2 r_2^2 e^{-4\alpha L} + 2 r_1 r_2 e^{-2\alpha L}} = \frac{t_1^2 t_2^2}{(1+A)^2} \quad \text{---(31)}$$

From Equations 30 and 31, ‘A’ can be represented as

$$A = \frac{\sqrt{\frac{T_R}{T_A}} + 1}{\sqrt{\frac{T_R}{T_A}} - 1} \,. \qquad \text{---(32)}$$

Taking natural logarithm of Equation 29,

$$\ln(A) = -2\alpha L + \ln(r_1 r_2) \,. \qquad \text{---(33)}$$

Length (cm)	1.1	1.74	2.34	2.9
ln(*A*)	-2.7095	-3.3451	-3.1575	-3.333

Table 4: Natural logarithm of amplitude of maximum oscillation from different graphs (Figure 32-35) is tabulated. All waveguides are 10µm wide.

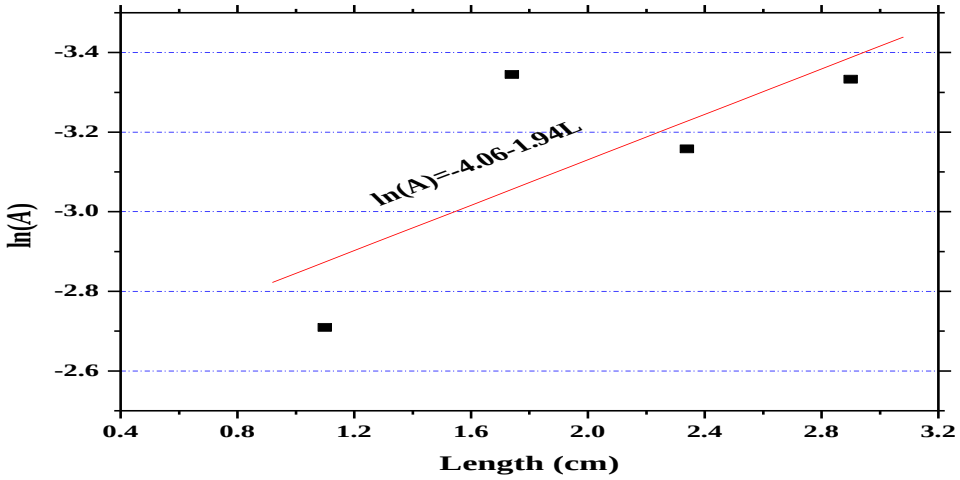

Figure 36: Graph shows linear regression of *ln*(*A*) vs cavity length *L* in a 10µm wide waveguide. The slope -2α is – 1.94 **and *ln*(r_1r_2) is - 4.06 (Equation 33).**

From linear regression (Figure 36) it is visible that slope -2α is – 1.94. Thus, the value of coefficient of attenuation is calculated to be 1.52dB/cm for 10µm wide waveguides. If equal reflectivity of two facets is assumed, then 31.2% of the incident light is reflected at each facet (Equation 29).

The amplitude of maximum oscillations from the Figure 32 to 35 decreases with increasing length. This behavior is in confirmation with theory, as distance between mirrors increases the attenuation of signal should also increase. Using the same argument, it may be stated that output power increases with decreasing length of the waveguide as

shown in Figure 37, series 1 is an exception, which may be attributed to irregular facets (Table 1).

Error Analysis

R^2 value for data in Table 4 and Figure 36 is 0.99 for three point-optimized curve.

Theoretically, maximum value of loss can be predicted by inserting maximum value of reflectivity of the facets in Equation 29.

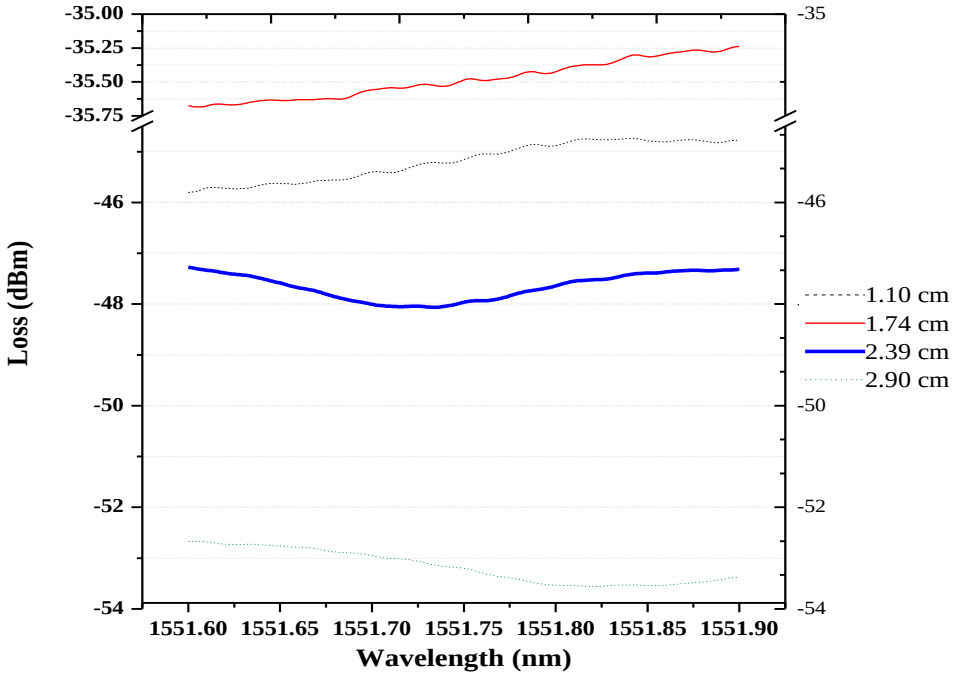

Figure 37: Combined plot of Figure 32-35. 100-point adjacent averaged data points in the wavelength range 1551.6 to 1551.9nm. Graph has a break at -44dBm until -35.75dBm. Average value of output power increases with decreasing waveguide length.

$$r_{\max} = (n_{eff} - n_{air})/(n_{eff} + n_{air}) \qquad \text{---(34)}$$

n_{eff} is effective index of the waveguide. Material index value of 3.65 (at 1.55µm) measured by ellipsometry (Figure 17) is used in simulation of the waveguide modes by Fimmwave, Ver. 4.3. n_{eff} obtained for the fundamental TE mode is 2.93 and corresponding reflectivity is 49%. Maximum value of α obtained is 5.28dB/cm for a 10µm wide waveguide. This loss estimate is maximum summation of scattering, radiation and material absorption.

Bragg Mirror

The loss estimated above appreciably depends on reflectivity of the facets thus to have high amplitude oscillations in the spectrum bragg mirrors were fabricated at one end of the waveguide.

Bragg mirror is fabricated near one of the waveguide facets by e-beam (electron beam) lithography followed by RIE. There are 250 grooves with constant period of 300nm and etch depth of 30nm. SEM image of the grooves is shown in Figure 38. In Figure 39 spectrum of 7µm wide waveguide with a tunable laser source is shown. Using Equation 33 Bragg mirror reflectivity is estimate.

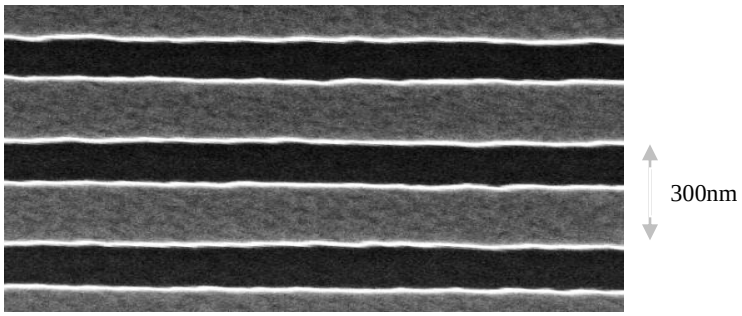

Figure 38: SEM image of the gratings, period of the gratings is confirmed from this image. The region of lower brightness is about 100nm trench and brighter region is un-etched about 300nm wide.

Two cavities result from the fabricated Bragg mirror. However, oscillations from shorter cavity are easily observable, since its period and amplitude of oscillation is much larger. Since loss in longer lengths is higher, amplitude of oscillation in larger cavity is weaker. Weak high frequency oscillations superimpose on wider high amplitude oscillations in the transmission spectra. Using the following results from previous discussion-

α_{max}=6dB/cm, α_{min}=1.5dB/cm, $r_{facet\ min}$=0.31,$r_{facet,max}$=0.49

Length of the shorter section is 0.1cm and *ln(A)* is obtained from Figure 39. As a result, reflectivity of the fabricated Bragg mirrors lies in the range 49 to 86%.

3.3. Spectral Behavior

The spectral analysis of an optical component characterizes its behavior with respect to wavelength. Following analysis is of much significance because important parameters like effective index, V-number are functions of wavelength (Equation 22).

Procedure

Fiber-to-fiber measurement is conducted to ascertain the inherent loss in the setup. This step is carried out before analyzing the spectrum and also after completion of the measurements to ensure that there are no awry readings. The setup as shown in the schematic (Figure 41) is used for the experiment.

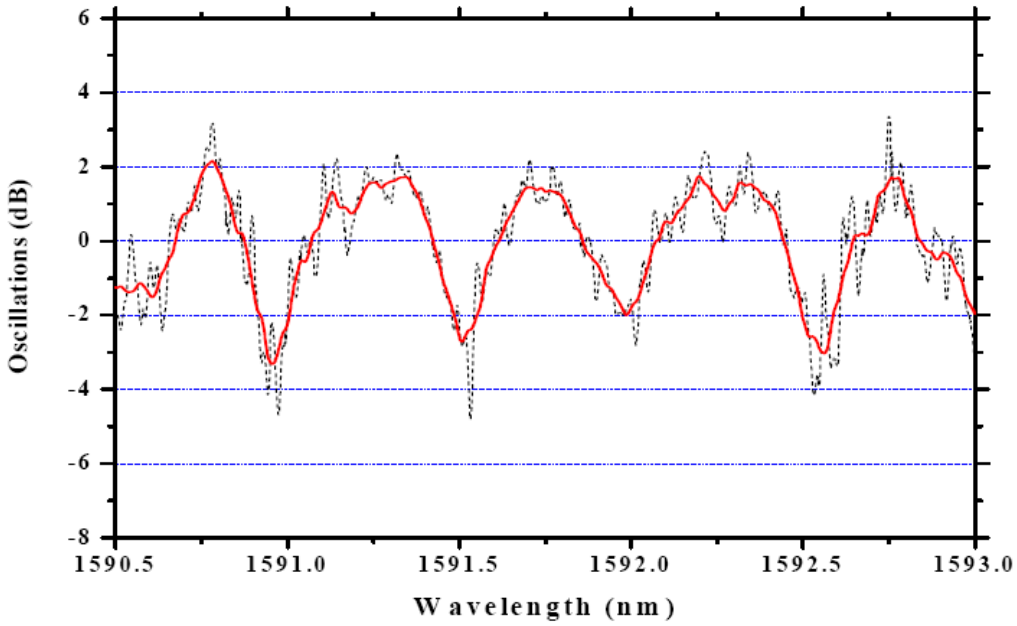

Figure 39: Fabry-Pérot oscillation spectrum of a 7µm wide waveguide with Bragg Mirror fabricated 1mm from one end-facet. The dotted line represents the measured spectrum and the solid line is the fitted curve. Smaller period oscillations result from the longer cavity of approximate length 1.4cm. These smaller oscillations are superimposed over larger period higher amplitude oscillations from 1mm length cavity.

Source Details

Highly non linear fiber (HNLF) is designed to enhance non-linear effects that cause the spectrum to broaden the spectrum of light. Four Wave Mixing, Self-Phase Modulation, Stimulated Raman Scattering all contribute to supercontinuum generation. The span of the continuum generated is related to the wavelength of the laser light and the dispersion properties of the HNLF. These dispersion properties can be precisely controlled to allow supercontinuum generation at different wavelength spans. Super continuum is generated by coupling the radiation at 1064nm from a miniature Q-switched laser into a highly non-linear photonic crystal fiber. Result is a broadband spectrum extending from 600 to 1800nm. Spectrum is analyzed from 1300 to 1750nm. The super continuum setup is

extremely sensitive to its surrounding and thus care has to be taken to keep the optical bench steady.

Results

Fiber to fiber power of –23dBm is noted during measurements, this is taken as a reference before aligning any waveguide. The spectrum of super continuum is almost a constant at –23dBm for the fibers. However, all the waveguides irrespective of length show a band pass behavior between 1500 to 1700nm.

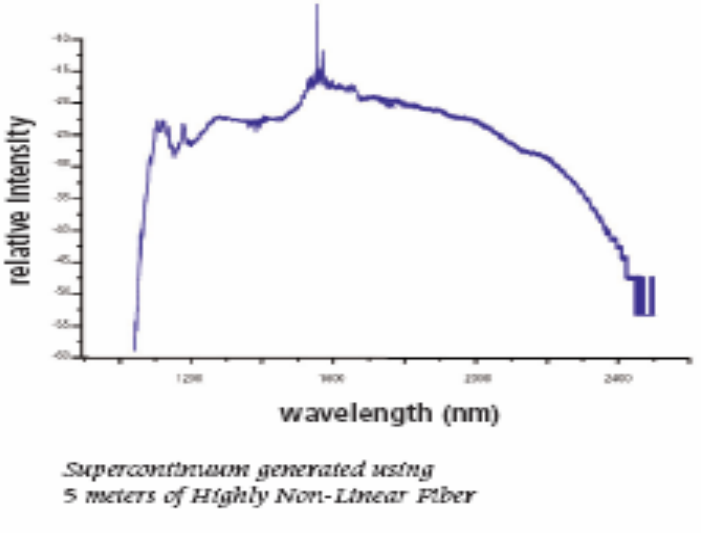

Figure 40: Wideband spectrum generated by the supercontinuum source from 1200 to 2400nm.

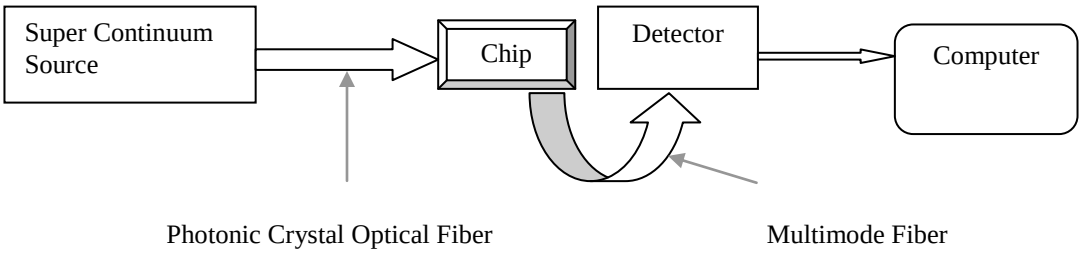

Figure 41: Schematic of the spectrum analysis setup.

Plot details

For distinctly analyzing the data, first, power in dBm has been converted into milliwatts and then averaged for ten successive points. After averaging, power is reconverted into dBm for compression of *y* coordinates and subsequent smoothening of the graph as shown in Figure 42 and 43.

Error Analysis

Error in the spectral analysis could be because of mis-alignment in the fiber and the waveguide, which is independent of measurement procedure. However, one significant concern could be the highly sensitive source. The setup of the supercontinuum is extremely sensitive to the surrounding and minor perturbations. This though cannot be estimated except by measuring the source power before and after the experiment. In this experiment the power level before and after the experiments were same and thus it may be assumed that the source has not led to errors.

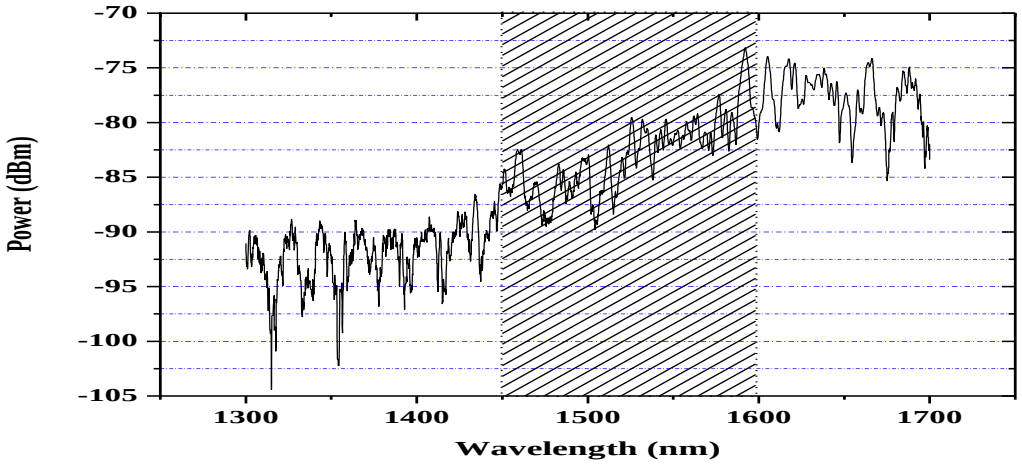

Figure 42: Waveguide length *L*= 2.9cm. Improving transmission for wavelength 1450 to 1600nm is observed. Oscillations may be attributed to the mirror-like behavior of the facets.

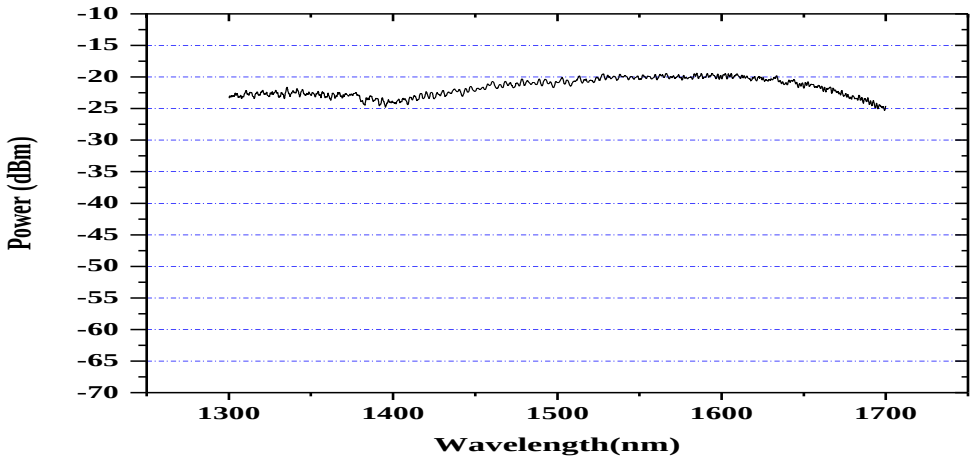

Figure 43: Fiber to fiber spectrum is almost constant showing no variation for the different wavelengths.

Discussion

The losses in a-Si:H strip optical waveguides are low and the results are comparable to the best reported in the scientific community so far. However, reproducibility and a more reliable method for measurement needs to be established.

In Figure 40 a pattern of increasing transparency can be attributed to the optical properties of a-Si:H –

1) From the wavelength range 1450 to 1600nm output power increases. In thin film materials Urbach-energy *Eu* is related to small values of attenuation (α). It is found that the α(E) spectrum displays an exponential relation. A fit of *E* versus α data to an exponential function [23, 24]

$$\alpha(E) = \exp(-Eu/E), \qquad \textbf{---(34)}$$

yields the Urbach energy *Eu* . In good quality a-Si:H films the value is around 50meV, but it may increase up to 250meV. While other optical functions depend mostly on the film composition, the Urbach energy is strongly disorder dependent.

According to Equation 34 $\alpha(E) \propto E$. **---(35)**

Since $E \propto \lambda^{-1}$ therefore $\alpha(\lambda) \propto \lambda^{-1}$. **---(36)**

As α decreases the value of output power from the waveguide should increase, which is verified by our results. Oscillations that are visible in the graph (Figure 32) occur due to resonance of allowed modes (Equation 9).

2) Roughness of the structure may also contribute to the observation that higher wavelengths exhibit higher transparency. This may be because of comparable dimensions of roughness and small wavelengths, leading to greater scattering at lower wavelengths.

3) Absorption-tail could be another reason why higher wavelengths exhibit lower absorption.

4. SOI Devices

4.1. Etched Mirrors

The mirrors have been fabricated on SOI (silicon on insulator) substrate. The device is easy to fabricate- top layer silicon is semi-etched to fabricate the waveguide cladding and fully etched to fabricate the mirrors.

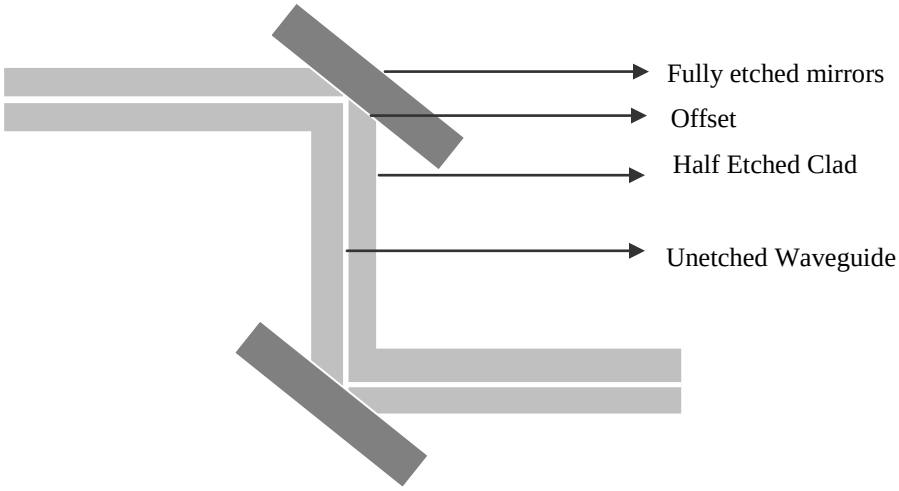

Figure 44: Top view of section of two mirrors altering the path of light by 90˚ each.

Specifications

Width of silicon waveguide section is 3.7μm on the mask and its refractive index is 3.48. Height of the waveguides is 4μm. The mirror section has an offset from the waveguide which is almost zero in the figure above. Positive offset implying increasing distance from the waveguide.

Procedure

Ends of the waveguides are aligned with polarization maintaining optical fiber at input and other end of the waveguide is aligned with a single mode optical fiber. Index matching oil is used to avoid reflections from the facets. Power levels through different configurations involving different number of mirrors is measured and used to analyze loss per mirror section for the TE and the TM mode. Mirrors with offset of 200nm and 400nm are also measured.

N	Mode	O = 0nm	O = 200nm	O = 400nm
0	TM	-16.8	-17.05	-16.93
	TE	-17.7	-18.11	-17.72
4	TM	-19.1	-19.58	-20.2
	TE	-20.7	-21.16	-21.7
8	TM	-21.07	-22.15	-23.66
	TE	-24.18	-25.06	-25.88
12	TM	-24.6	-24.47	-26.7
	TE	-28.6	-28.59	-29.5
16	TM	-26.02	-26.9	-31.9
	TE	-31.02	-31.7	-35.1
20	TM	-27.4	-29.9	-34.5
	TE	-33.44	-36.1	-38.02

Table 5: N refers to number of mirrors in the waveguide, and O is the offset in nanometers. The data is measured power level for the TE and the TM modes.

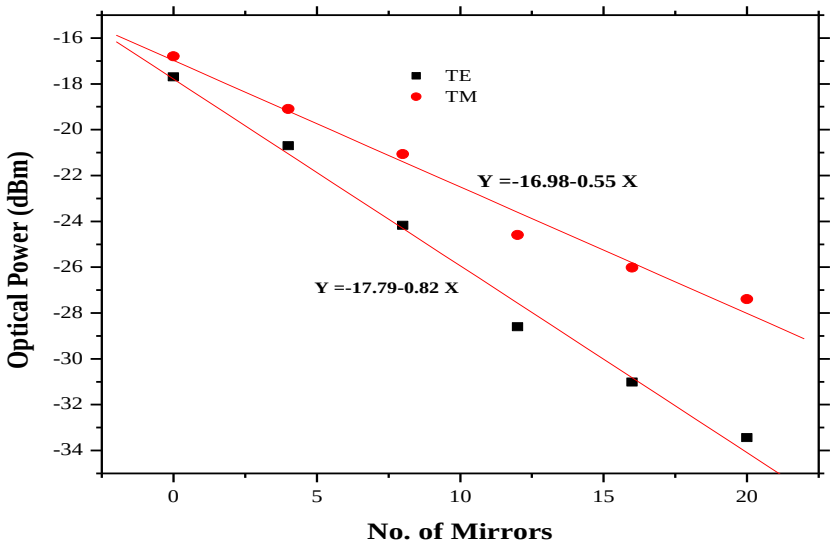

Figure 45: O=0nm, TE mode has loss is 0.82dB and TM mode 0.55dB, per mirror section.

Loss per mirror section is minimum for no offset. Higher loss in the TE mode as compared to the TM mode could be on account of the modes interacting with different etch dimensions of the mirror.

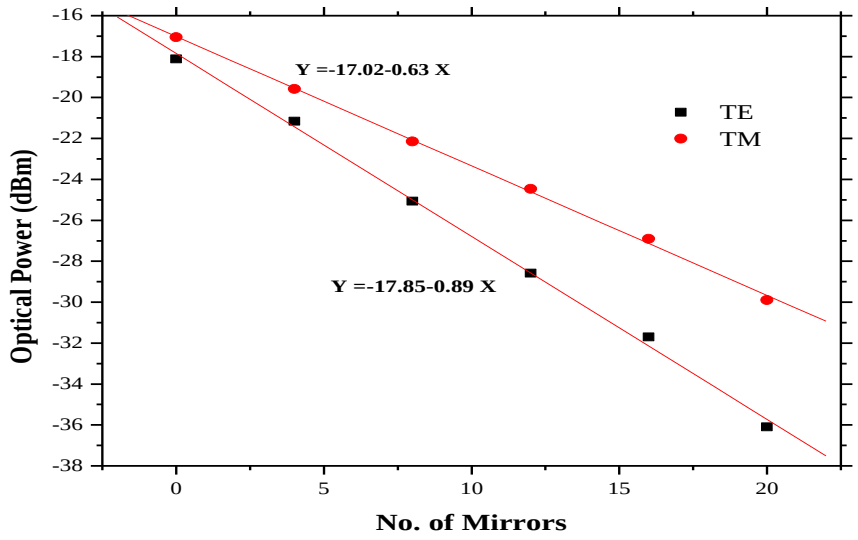

Figure 46: O=200nm, TE mode loss is 0.89dB and TM mode loss is 0.63dB per mirror section.

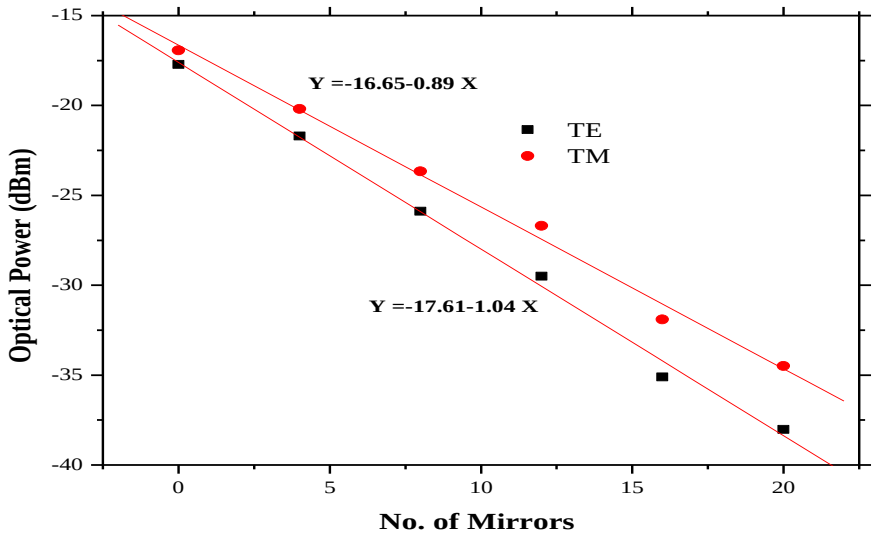

Figure 47: O=400nm, TE mode loss is 1.04dB and TM mode loss is 0.89dB per mirror section.

Offset (nm)	TE (dB/mirror section)	TM (dB/mirror section)
0	0.82	0.55
200	0.89	0.63
400	1.04	0.89

Table 6: Results of measurements for different offsets for TE and TM modes in db/mirror section.

4.2. Rib Waveguides

The rib waveguide is schematically shown in Figure 6c. Measured waveguide has width of 4µm height of 6µm and etch depth of 50%. Loss is measured by the Fabry-Pérot method (p 23).

Loss

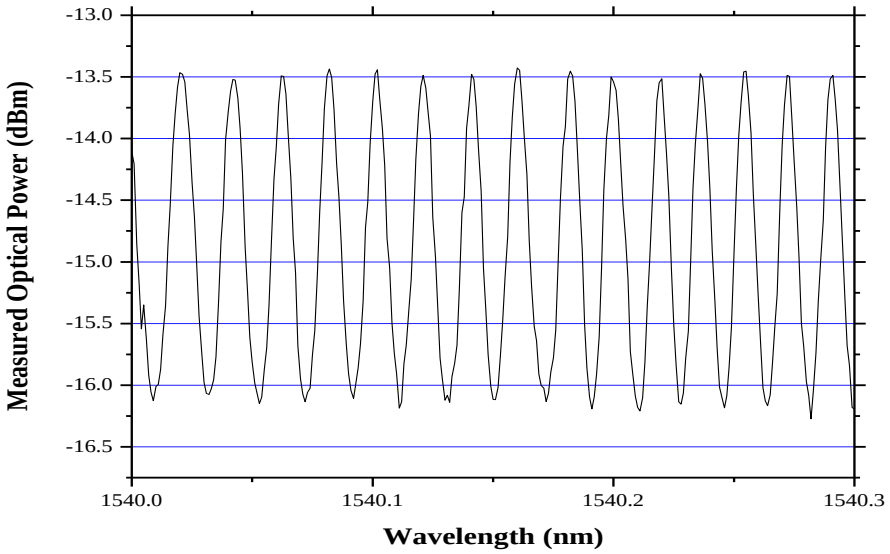

Figure 48: Oscillation Spectrum for a 1.1cm long rib waveguide of width 4µm height 6µm and etch depth of 50%, O=2.7dB.

Theoretical value of reflectivity is 40% (using refractive index of oil as 1.5 and silicon as 3.48). Using Equations 26-33, the estimated value of loss is 0.1dB/cm.

Birefringence

Polarization state of light propagating in a standard single mode fiber is random. Consequently a polarization independent performance is desirable for an optical waveguide device used in an optical fiber system or network [32]. Thus the measure of birefringence within the waveguide is of paramount importance during its characterization.

Birefringence is defined as the difference between the group indexes along orthogonal axes of propagation within the fiber. Single mode propagating within the waveguide constitutes orthogonal TE and TM polarizations. If the waveguide is anisotropic then the two polarizations would travel with different group indexes. The differing group indexes lead to dispersion as demonstrated in Figure 49.

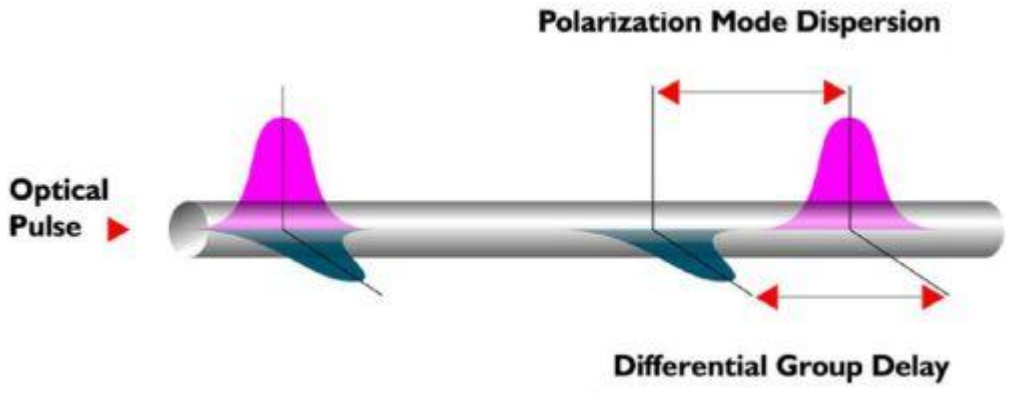

Figure 49: Illustration of birefringent media leading to polarization mode dispersion.

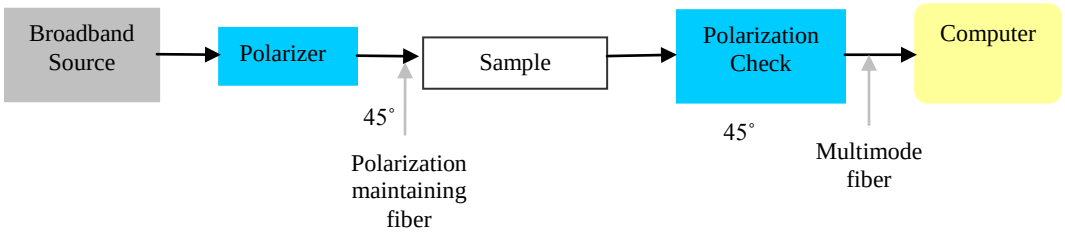

Figure 50: Schematic of the measurement setup used for measuring birefringence.

Broadband source is used; the linearly polarized light is filtered from the polarizer, oriented at 45˚ and coupled to the waveguide sample from a polarization maintaining fiber. Index matching oil is used to prevent reflections. At the output of the sample, light at 45˚ is filtered through a prism. Spectrum of this light is analyzed.

Waveguide birefringence induces a periodic transmission curve as a function of frequency. The period is equivalent to one beat length (2π).

$$\Delta n = m * {}^{c}\!/\!_{(\Delta f * l)} = m * {}^{(\lambda_1 * \lambda_2)}\!/\!_{(\Delta\lambda * L)} \qquad \text{--- (37)}$$

Where 'm' is the number of periods included in the frequency range Δf and L is the length of the waveguide.

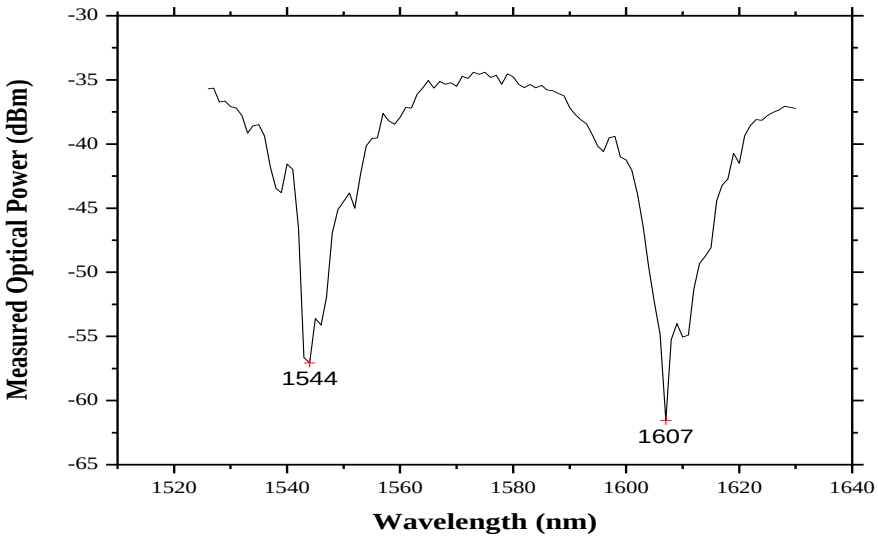

Figure 51: One period of the oscillation spectrum. To find the period of oscillation the peaks shown are used.

Birefringence from the above spectrum is obtained to be $4*10^{-4}$ (Figure 51). Simulations using Fimmwave show the difference in group indexes of the fundamental TE and the TM mode of the waveguide (Figure 52) to be $4.7*10^{-3}$. One possible reason for higher birefringence in using the software could be the consideration of only the fundamental modes during simulations. The measured birefringence is about ten times higher than recently reported low birefringence in similar SOI waveguides, where the waveguide dimensions have been optimized [33].

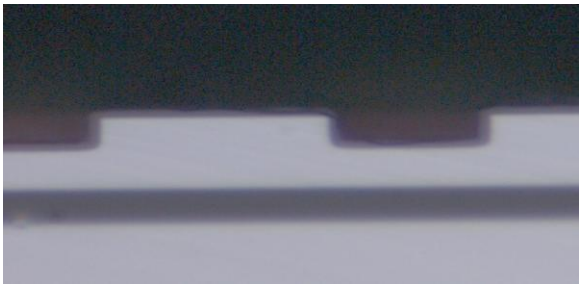

Figure 52: Rib waveguide 6µm wide, 2µm high with etch depth of 50%.

5. Improvements

Coupling Losses

The statistically estimated values of coupling losses are much higher than the material or functional loss in the waveguide (p 23). This loss can be reduced by using tapered waveguide ends or tapered fibers or both.

Cleaving

Diamond cutter is used to cleave the facets. An improved cutting method could much improve the coupling of light into and out of the waveguides. The inclination of facets leads to reflections and thus poor coupling. Reflections maybe reduced by the use of index matching oil.

Polishing

To smooth the facets polishing is done. Chemical mechanical Polishing (CMP) has been used for the SOI samples but for a-Si:H samples it is not done.

An Integrated Light Source [28]

It would be an elixir of sorts if an integrated light source could be fabricated on the chip, this would remove most of the optical coupling losses and other external hazards. Although process optimization is being carried out by various commercial enterprises like Intel and IBM, what needs to be found from the inventions perspective is a light source, which can be monolithically integrated with the waveguides. Before such a source, a modulator or wavelength conversion scheme employing lasers could completely transform the electrical signal to light on one chip and maybe further processed using light switches. This would provide the best use of the optical domain for fast computation and interconnection.

6. Conclusion

Methods to ascertain loss in optical waveguides have been employed and investigated. Strip a-Si:H waveguides and rib SOI waveguides of different cross sections are studied. Cut Back method and the Fabry-Pérot method have been used for measuring loss in the waveguides. The loss reported by Cut Back method s 3.89dB/cm and upper limit of loss by Fabry-Pérot method is 1.52dB/cm for a 10µm wide waveguide. This value of loss is comparable to the best reported in the scientific community so far. Cut Back method's reliance on coupling efficiency makes it an arduous and less predictable method. However, grating couplers could be used for Cut Back analysis in future. The Fabry-Pérot method has a distinct advantage that minor misalignments in coupling light into the waveguides do not affect the end result at all.

A significant advantage of strip waveguides fabricated by PECVD is their ease of compatibility with the CMOS process. Although whimsically, it maybe envisaged that such a layer of optical components might be deposited over conventional mass produced electronics in future, to achieve improved functionality, faster processing, more dense structures and vertical stacking of devices; overcoming the electronic bottlenecks like interconnect delay (1). Metaphorically, a-Si:H is like plasticine – not having a long-range crystal order, easily deposited over any material and for a different reason is most significant because of its optical transparency at the communication wavelength.

SOI waveguides have also been analyzed by the Fabry-Pérot method; reported loss in a 4µm wide rib waveguide is 0.1dB/cm. The losses in SOI optical waveguides are much lower than a-Si:H because rib waveguides are less sensitive to surface roughness, there are no dangling bonds and sustained investment to optimize fabrication techniques.

It is pivotal to mention that waveguides alone can be used in devices requiring signal transmission like in communication systems. However, if light sources and modulators are integrated on the chip then their applications for hybrid opto-electronic circuits may also be realized. Large corporations have ongoing research programs to develop such a light source and integrate it to the waveguides. For this purpose, high reflectivity Bragg mirrors have been fabricated onto a-Si:H strip waveguides by e-beam lithography. The

estimated reflectivity of such a mirror is approximately in the range 49-86%. In future InP could be bonded over such a short (tens of micrometers) cavity comprising two Bragg mirrors in hope to observe lasing.

In SOI waveguides a method to analyze birefringence is also studied and the value of measured birefringence is $4 * 10^{-4}$. Finally, another passive device, etched mirrors on SOI chip have been analyzed for loss per section corresponding to TE and the TM modes by the Cut Back Method.

Parts of the results obtained have been presented in an international conference (P. 51). With the completion of this thesis work a foundation for studying more complex structures has been laid. In future, structures like tapers, Y-Junctions, slot waveguides, ring resonators on a-Si:H may also be investigated. Thermo optical modulators, all optical regeneration and integrating strip waveguides with ion exchanged glass waveguides for light confinement in the vertical direction are also promising research domains.

Cumulatively, through the period of research leading to the completion of the Masters thesis the sphere of Silicon Photonics has been studied, practiced and hopefully comprehended.

7. Publication

The research carried out as part of this Masters thesis work has been accepted for publication.

International Conference Paper

Title: Amorphous silicon optical waveguides and Bragg mirrors

Authors: Amit Khanna, Mikaël Mulot, Sanna Arpiainen, Antti Säynätjoki, Jouni Ahopelto, Seppo K. Honkanen, Harri K. Lipsanen

Proceedings of SPIE Volume 6996
Paper 6996-4

The paper is part of international conference 'SPIE Photonics Europe' in Strasbourg, France. A talk was presented on 7th April 2008 in the session on Photonic Integrated Circuits and Silicon Photonics.

8. Appendix I

Instruments and Manufacturers

Detector InGaAs:	Light Wave Multimeter, Hewlett Packard, 8153A
Portable Coarse light Detector:	FotecM
Tunable Laser:	Tunable external Cavity laser, Photonetics
Mount for Fibers:	NanoMax, Milles Griot
Lamp:	Schott Mainz KL150B
EDFA power supply:	TTi (Thurlby Thunder instruments)
Microscope:	0.7x-3x, Bausch and Lomb
Prism for Polarisation Check:	Ealing
Super Continuum:	Laser and Peltier driver
Optical spectrum Analyser:	AQ6317, Ando
Platform and Mount base:	THOR LABS

9. References

[1] G. Cocorullo, et al.....IEEE Jour Quant Electr Vol4, No.6, Nov/Dec 1998.

[2] J. S. Foresi, et al…… Appl Phy Lett Vol68,No.15, Apr 1996.

[3] Werner J. et al…… .Appl Phy Lett Vol53, No.16, 1988, pp 1693.

[4] R. J. Walker…….……Electron Lett Vol21, 1985, pp 581.

[5] P. K. Tien……...…Appl Optics, Vol10, No.11, 1971, pp 2395.

[6] Marc D. Himel, Ursula J. Gibson….Appl Optics, Vol25, No.23, 1986, pp 413.

[7] Y. A. Kao and T. Miyazoki……..Maruzen, Tokyo, 1981.

[8] A. Säynätjoki, et al……...J Opt A: Pure Appl Opt 8 (2006) S502-S506.

[9] L .C. Kimberling……..Devices for Silicon Microphotonic Interconnection.

[10] Atsushi Sakai et al……Jpn J Appl Phy, Vol40, No.4b, 2001.

[11] Website……www.wikipedia.org .

[12] R..Orobtchouk et al……..Proc of SPIE,Vol6183 618304-2, 2006.

[13] Matteo Dainese…….…Plasma Tech. Si based PICs, Doctoral Thesis KTH, Stockholm, 2005.

[14] Liu Liu…….…Doctoral Thesis in Microelectronics and Applied Physics, KTH, Stockholm, 2006.

[15] R. A. Song, J. P. Lorenzo…….IEEE J Quant Electron, QE-22, 1986, pp 873.

[16] OnlineTool:1D mode solver…….www.home.math.utwente.nl/~hammer/oms.html

[17] Yahuda B. Band……Interaction of light and Matter .

[18] M. J. A. de Dood et al……..……...J Appl Phy, Vol92, No.2, 2002.

[19] S. O. Kasap…….....Optoelectronics and Photonics, Prentice Hall, 2001.

[20] Gerd Kaiser……...Optical Communication, MacGraw Hill, 2000.

[21] K. J. Ebeling……....Integrated Optoelectronics, Springer Verlag, 1993.

[22]Kimmo Solehmainen…….Doctoral Thesis, Fabrication of Microphotonic Waveguide Components on Silicon, VTT, 2007.

[23] Tim Searle……Properties of Amorphous silicon and its alloys, Institute of engineers and technology, 1998.

[24] G. D. Cody et al……Disorder and Optical absorption edge of Hydrogenated Amorphous Silicon, Phs Rev Lett Vol47 No.20, 1981.

[25] S. E. Miller, Integrated Optics: an introduction,..*Bell Syst. Tech. J.*, vol. 48, p. 2059, 1969.

[26] On-Chip Copper-Based vs. Optical Interconnects: Delay Uncertainty,Latency, Power, and Bandwidth Density Comparative Predictions…Guoqing Chen et.al.

[27]Website (smallest projector in the world)- http://www.tfot.info/articles.php?itemId=48/59/ .

[28] Tuomo von Lerber …….Applications of fiber optical resonators in measurement and telelcommunications technology (Doctoral Dissertation), TKK, 2007.

[29] S. Muraleedharan …….GaN blue LEDs (Masters Theses), 2007.

[30] Y.H. Kim,…….. Large-grain polycrystalline silicon film by sequential lateral solidification on a plastic substrate, Thin Solid Films Volume 493, Issues 1-2, 22 December 2005, Pages 192-196.

[31] A.Saynatjoki……Optical waveguides on polysilicon-on-insulator, Journal of Material science, 14, 2003.

[32]Daoxin Dai and Sailing He……..Analysis of birefringence of a SOI rib waveguide, Applied optics, Volume 43, No. 5.

[33] Shih-Hsiang Hu……5µm thick waveguide with low birefringence and low roughness and optical interconnection using high numerical aperture fiber, IEEE Photonics Tech. Lett., Volume 20, No.12.

[34] www.rp-photonics.com

[35] http://www3.imperial.ac.uk/portal/

[36] www.eere.energy.gov

[37] A Harke et.al…….. Low-loss single mode amorphous silicon waveguides, Elec. Lett. 2005, Volume 41, No. 25.

[38] Seppo Honkanen…….Lecture slides, Photonics and Integrated Optics, TKK Autumn 2007.